https://dx.doi.org/10.1016/j.tws.2021.108792

Design for local buckling behaviour of welded high strength steel I-sections under bending

Shuxian CHEN[1]; Han FANG[2]; Jun-zhi LIU[1]; Tak-Ming CHAN[1]*

1 Department of Civil and Environmental Engineering, The Hong Kong Polytechnic University, Hong Kong, China

2 School of Civil, Environmental and Mining Engineering, The University of Adelaide, South Australia 5005, Australia

* Corresponding author: tak-ming.chan@polyu.edu.hk

Abstract

Local buckling behaviour of welded high strength steel (HSS) I-sections subjected to bending is crucial for structural designs, and has been found to be affected by the interactive effect between flanges and web. To realise accurate designs considering the local buckling behaviour, the continuous strength method (CSM), direct strength method (DSM) and the method from Kato, all of which incorporate the element interaction, have been developed for hot-rolled or cold-formed structures fabricated with conventional strength steel, aluminium or stainless steel. This paper aims to extend these methods for the design of welded HSS I-sections subject to bending. The results of 593 HSS material tensile tests and 40 tests on HSS I-beams are collated. 526 numerical models are generated to expand the data pool for this study using the validated finite element method. Underpinned by the collection of test data and numerical data generated from an extensive parametric study, the design expressions based on the CSM, DSM and the method from Kato, applicable to HSS I-sections under bending, are proposed. The statistical and reliability analysis indicate that the proposed CSM, DSM and Kato's method provide more satisfactory strength predictions than the codified design rules in Eurocode 3 and AISC specification. In comparison with the proposed CSM and DSM, the predictions based on the modified Kato's method show higher accuracy, which may be attributed to the separate consideration for the effect of flange and web slenderness in Kato's expression.

Keywords: Local buckling behaviour; welded high strength steel I-section; bending; continuous strength method; direct strength method; the method from Kato.

1 Introduction

High strength steel (HSS), typically defined as the steel with nominal yield stress of more than 460 MPa [1-2], has attracted increasing attention for its application in the construction of buildings and bridges [3] due to its higher strength than conventional strength steel for lighter and stronger structures with reduced embodied carbon footprint [4]. To apply HSS structures in the engineering practice, efficient design methods of the structures are vital. For the design of HSS structures, local buckling behaviour is one of the main concerns due to its relatively thin plate thickness. The current codified design methods [5-6] developed primarily based on the research data for conventional strength steel structures use the concept of section classification to identify the extent which the cross-section resistance is limited by local buckling. Generally, in these specifications, the plate width to thickness limit of each class is provided individually for different plate elements. However, element interaction is experienced by the constitutive plates of section, as the degree of restraint against rotation at the junction of plate elements relies on the geometric characteristics of the joined plates. In the last two decades, the interactive effect between flanges and web in high strength steel (HSS) I-sections under bending has been highlighted by many researchers [7-12]. It is thus imperative to generate more efficient design methods for the design of local buckling of HSS I-beams.

Hitherto, the deformation-based continuous strength method (CSM), and the strength-based direct strength method (DSM) have been developed for predicting the cross-sectional resistance with the consideration of local buckling behaviour for structures fabricated with aluminium alloy [13-15], stainless steel [16-18], hot-rolled steel [19] and cold-formed steel [20-21] with various cross-section shapes. Both methods are based on the overall cross-section slenderness λ_p, instead of the slenderness of individual constitutive plates, so that element interaction can be taken into account. Owing to these advantages of CSM and DSM, research studies have been performed to extend the methods to HSS structures with tubular cross-sections and subject to compression or bending [22-24]. However, the suitability of CSM and DSM for HSS I-section subjected to bending remains unexplored, leading to the motivation of this study.

In addition to the CSM and DSM, a semi-empirical approach proposed by Kato [25-26] is well-established for dealing with the local bucking of I-section. In this method, a simple design expression incorporating both flange slenderness and web slenderness to inherently take the flange-web interaction into account is used to calculate local buckling resistance of members. This method has been adopted by Japanese limit state design of steel structures [27], and the slenderness limit for cross-sections made of Japanese conventional steels-SN 400, SN490 and SA 440 grade steels are specified in this code. Kato’s method was also utilized by Beg and Hladnild [7] to establish the Class 3 slenderness limit for I-beams made of HSS NIONICRAL 70 (nominal yield stress $f_{y,nom}$ =700 MPa) through a parametric study of 17 numerical models. However, this slenderness limit was developed using relatively limited test data. Thus, developing a reliable design expression based on the Kato’s method for HSS I-sections under bending is also considered in this study.

In this paper, test data on HSS tensile coupons and HSS I-beams were firstly gathered. A validated finite element method was subsequently employed to generate sufficient data covering various geometric dimensions and different HSS grades. Both the collated test results from the literature and the supplementary numerical data generated in this study were utilised to evaluate the existing CSM, DSM and Kato's method and to develop the modified expressions applicable for HSS I-beams. Improved accuracy of the proposed design methods for estimating the local buckling resistance of HSS I-section under bending was demonstrated through the comparison with the predictions using the codified design rules. The reliability of the proposed design methods was also examined by performing a reliability analysis in accordance with the European code approach [28].

2 Experimental database

2.1 Tensile Coupon tests for HSS

A total of 593 HSS tensile coupon test results were gathered to capture the basic material properties for developing the material model for HSS. The model was subsequently used for numerically investigating HSS structures and developing CSM for HSS I-sections under bending, as described in subsequent sections. Based on characteristics of the measured stress-strain curves reported in the literature, HSS materials were classified into three series, as listed in **Table 1**. The most remarkable distinction among these series is the yield plateau: curves of the steel with $f_{y,nom}$ = 460 MPa primarily have a distinct yield plateau, while the steel with $f_{y,nom}$ from 890 to 1100 MPa have a round material response with the absence of a well-defined yield point; for the steel with $f_{y,nom}$ = 500-700 MPa, both of the above cases have been observed. **Tables 2-4** summarizes the number and details of HSS test data for each series. The yield plateau and delivery condition for steels with $f_{y,nom}$ from 500 to 700 MPa are highlighted in Table 3 to identify the relationship between them, and no obvious relation was observed on the basis of the presented information in this table. The collected data in **Tables 2-4**, unless otherwise specified, were generated through testing coupons cut from steel sheets. In these tables, f and ε represent the stress and strain of steel material, respectively; ε_u means the ultimate tensile strain, and ε_{sh} is the strain at onset of strain hardening, as illustrated in the **Fig. 1**.

Table 1 Characteristics of the measured stress-strain curve for HSS materials

Nominal yield stress /MPa	Yield plateau
460	Y
500-700	B
890-1100	N

Note: “Y” represents that the yield plateau is observed in the engineering stress-strain curves; “N” represents no yield plateau is found; “B” means that both “Y” and “N” coexist for this case.

Table 2 Summary of tensile coupon test results for the steel with $f_{y,nom}$ = 460 MPa

Reference	Steel grade	Full f-ε curves	ε_u	ε_{sh}[a]
[29]	Q460C	/	2	/
[30]	Q460D	/	3	/
[31]△	Q460C	4	3	3
[32]	Q460C	/	3	3
[33]	Q460	/	2	2
[34]△	Q460D	3	3	3
[35]	Q460GJ	3	/	/
[36]	Q460	/	6	6
[37]△,[38]	S460 (SHS[b] and RHS[c])	1	6	/
[39-43]	Q460GJ	9	30	15
[44]	Q460D	2	3	/
[45]	Q460	10	/	/
[46]	Q460	3	3	3
[47]	Q460D	2	2	/
[48]	Q460GJ	2	2	/
[49]	Q460GJ	2	2	/
[50]	Q460GJ	2	2	2
[51]	Q460 (sheet and OctHS[d])	2	30	2
[52]	Q460C	5	/	/
	Total	50	102	39

/: the information is unavailable in the literature.

[a]: the value of ε_{sh} is given in the literature

[b]: square hollow section; [c]: rectangle hollow section; [d]: octagonal hollow section

Table 3 Summary of tensile coupon test results for the steel with $f_{y,nom}$ = 500-700 MPa

Reference	Steel grade	Full f-ε curves	ε_u	ε_{sh} [a]	Delivery Condition
[53]	A514	/	12	Y	QT
[54]	BISALLOY 80	2	2	N	QT
[55]	700Q	1	1	Y	QT
[56]	HPS-100W	5	5	B	QT
[11]	BISPLATE-80	2	23	N	QT
[57] △	S690	/	2	/	/
[58]	S700MC	/	3	N	TMCP
	S690QL1	/	1	Y	QT
[59]	RQT701	1	/	N	QT
[35]	Q550GJ and Q690GJ	2	/	N	/
[60]	S690	1	/	N	QT
[61]	Q550	5	/	B	/
[62]	Q690D	/	5	/	/
[63]	Q550	5	/	Y	/
[64]	Q690	1	5	Y	/
[45]	Q550	10	/	Y	/
[65]	Q690D	2	5	Y	QT
[37] △,[38]	S690 (SHS[b] and RHS[c])	1	5	Y	QT
[66]	S690	9	9	B	/
[67]	Q690	2	9	Y	/
[44]	Q690D	1	3	Y	/
[68]	S690	12	40	Y	QT
[69]	Q690D	3	9	B	/
[47]	Q550D	6	2	B	/
	Q690D	4	1	N	/
[70]	Q550	3	3	B	/
[71]	S690	5	5	B	QT
[72]	Q550	1	/	N	QT
	Q690	1	/	Y	

[73]	S690	2	6	Y	/
[74]	S690 (OctHS[d])	9	44	N	QT
[75]	S700MC	2	2	B	TMCP
[76]	BISALLOY 80 (Box and I-sections)	1	/	N	QT
[77]	S500	2	/	B	/
	S690	2	/	N	/
[78]	Q690	1	6	Y	/
[79]	S690	/	2	/	/
[80]	S700	/	1	N	QT
[81]	S690 (angle and channel sections)	12	18	N	/
[82]	BISPLATE-80	2	2	N	QT
[83]	S690	1	2	N	/
[84]	S700MC	2	/	N	TMCP
[85]	S690	5	30	Y	/
[86]	S690	1	3	N	QT
[87]	Q690	1	3	N	QT
[88]	S690QL	2	2	B	QT
[89]	S690	1	7	Y	QT
[90]	Q690	1	/	N	QT
[91]	Q690	1	1	N	QT
[92]	Q690	2	2	N	/
[93]	Q690	3	3	B	/
[94]	S690QL	4	2	B	QT
	Total	142	286		

/: the information is unavailable in the literature.

QT: quenched and tempered steel; TMCP: thermo-mechanical controlled steel

[a]: "Y" represents that the yield plateau is observed in the engineering stress-strain curves; "N" represents no yield plateau is found; "B" means that both "Y" and "N" coexist for this case.

[b]: square hollow section; [c]: rectangle hollow section; [d]: octagonal hollow section

Table 4 Summary of tensile coupon test results for the steel with $f_{y,nom}$ = 890-1100 MPa

Reference	Steel grade	Full f-ε curves	ε_u
[57] △	S960	/	2
[58]	S960 QL	/	3
[31] △	960 MPa (Nominal yield stress)	1	1
[95]	960 MPa (Nominal yield stress)	/	3
[96]	S960	1	/
[68]	S960	1	1
[45]	Q890	5	1
[47]	Q890D	2	2
[72]	Q890	1	/
[97]	S960QL	2	2
[98]	S960	3	/
[80], [99]	S960 and S1100	2	4
[100]	Q960	3	/
[101]	S960 (sheets and channel sections)	1	8
[102]	Q960	1	3
[91]	Q960	1	1
[82]	BISPLATE-100	2	2
[92]	Q960	1	1
[103]	S960	4	2
	Total	31	36

/: the information is unavailable in the literature.

A statistical analysis of f_y /$f_{y,nom}$ and f_y /f_u was carried out based on the available tensile test results for measuring the properties of HSS, where f_y is the measured yield stress or 0.2% proof stress and f_u represents the ultimate tensile stress. The statistical results with the number of material test results are presented in **Table 5**. As can be seen in this table, it is obvious that fewer coupon tests on steel with $f_{y,nom}$ = 500-550 MPa and $f_{y,nom}$ = 960-1100 MPa have been conducted than those for steel with $f_{y,nom}$ = 460 MPa and $f_{y,nom}$ = 690-700 MPa. Generally, f_y is greater than 1.1 times $f_{y,nom}$, except for the steel with $f_{y,nom}$ = 960-1100 MPa, whose mean value of f_y /$f_{y,nom}$ ratios is 1.041 with CoV is 0.043. In terms of yield-to-tensile ratio f_y /f_u, the steel material with $f_{y,nom} \geq$ 690 MPa (the mean ratio is around 0.93) have lower values than those of the steel with $f_{y,nom}$ =460 MPa (the mean ratio is 0.819) and $f_{y,nom}$ = 500-550 MPa (the mean ratio is 0.885).

Table 5 Statistical analysis of HSS tensile coupon test results

$f_{y,nom}$ / MPa	$f_y / f_{y,nom}$		f_y / f_u		Number
	Mean	CoV	Mean	CoV	
460	1.133	0.070	0.819	0.057	131
500-550	1.237	0.059	0.885	0.038	49
690-700	1.110	0.046	0.933	0.028	348
960-1100	1.041	0.043	0.931	0.039	65

CoV: Coefficient of Variation

2.2 Summary of tests on HSS I-sections subject to bending

The reported experimental results of HSS I-beams, with failure mode of either yielding or local buckling, were collected, as listed in **Table 6** for this research. The steel grade, measured yield stress or 0.2% proof stress f_y, yield-to-tensile ratio f_y/f_u, overall cross-section slenderness λ_p and the number of available test specimens in the literature are also tabulated herein. The expression of λ_p is indicated by Eq. **(1)**, where σ_{cr} represents the elastic buckling stress. M_{el} is the elastic moment capacity, and M_{cr} means the elastic critical buckling moment under the boundary condition of tests. The listed yield-to-tensile ratios were corresponded to the constitutive plate element of I-section with a higher value of f_y/f_u. Despite that a wide range of steel yield stress (from 576 to 1003 MPa) and overall cross-section slenderness λ_p (from 0.27 to 0.95) were covered, the number of available test data is limited. Therefore, numerical method was utilized to supplement the data for this study.

$$\lambda_p = \sqrt{\frac{f_y}{\sigma_{cr}}} \text{ or } \sqrt{\frac{M_{el}}{M_{cr}}} \quad (1)$$

Table 6 Summary of experimental results for HSS I-beams

Reference	Steel grade	f_y/f_u	f_y /MPa	λ_p	Number
[104]	HSLA-80	0.88-0.91	576-609	0.27-0.61	4
[56]	HPS-100W	0.89-0.97	685-858	0.34-0.85	7
[11]	BISPLATE80	0.94	700-765	0.76-0.95	4
[105]	HSB800	0.95	991	0.63	1

	HSA800	0.90-0.94	903-956	0.30-0.77	3
[106]	S690	0.94	703	0.31-0.63	6
[82]	BISPLATE-80	0.93	791-851	0.64	1
	BISPLATE-100	0.94	998-1003	0.68	1
[93]	Q690	0.94	754-781	0.31-0.57	13
			576-1003	0.27-0.95	40

3 Finite element modelling

3.1 Finite element models

A commercial numerical analysis software-Abaqus 2019 was used to conduct finite element (FE) simulation for HSS I-beams. Full span models were firstly established to replicate the test conditions, while pure bending models were validated and employed in the subsequent parametric study. The element type-S4R, a four node, quadrilateral, stress/displacement shell element with reduced integration, was used to simulate the HSS I-sections. The mesh size was selected to be equal to the plate thickness after sensitivity analysis to obtain the balance between accuracy and computational cost. For the steel materials, the true stress-strain curve of steel materials converted from the engineering counterpart was used, and the multi-linear constitutive models displayed in **Fig. 1** were selected to describe the stress-strain relationship. In this figure, ε_y means the yield strain.

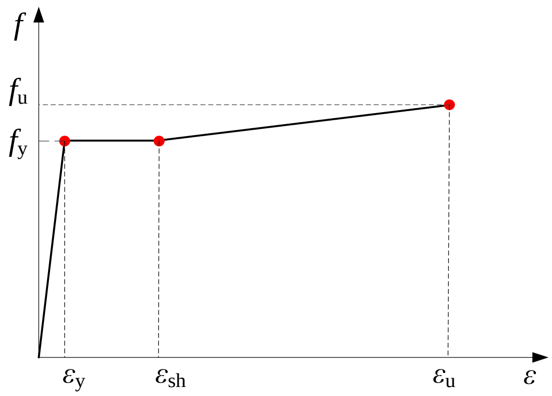

(a) The steel with a well-defined yield point

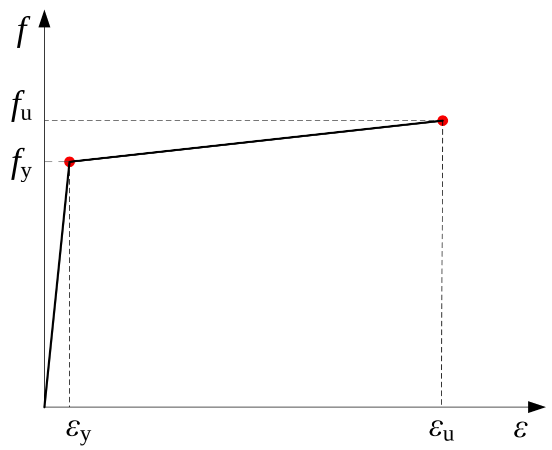

(b) The steel without a well-defined yield point

Fig. 1. Multi-linear stress-strain models for HSS applied in numerical simulation

Full span model was simply supported at two end supports with loading plates over the top flange, and the displacement was applied at the surface of loading plates, as displayed in **Fig. 2(a)**. The boundary condition of pure bending model is shown in **Fig. 2(b)**: each end section was connected to a concentric reference point (RP) through rigid body constraints; all degrees of freedom of RPs were constrained except for major and minor axis rotations at two ends and the longitudinal translation at one end; the forced rotations with identical value but opposite direction were applied at two ends.

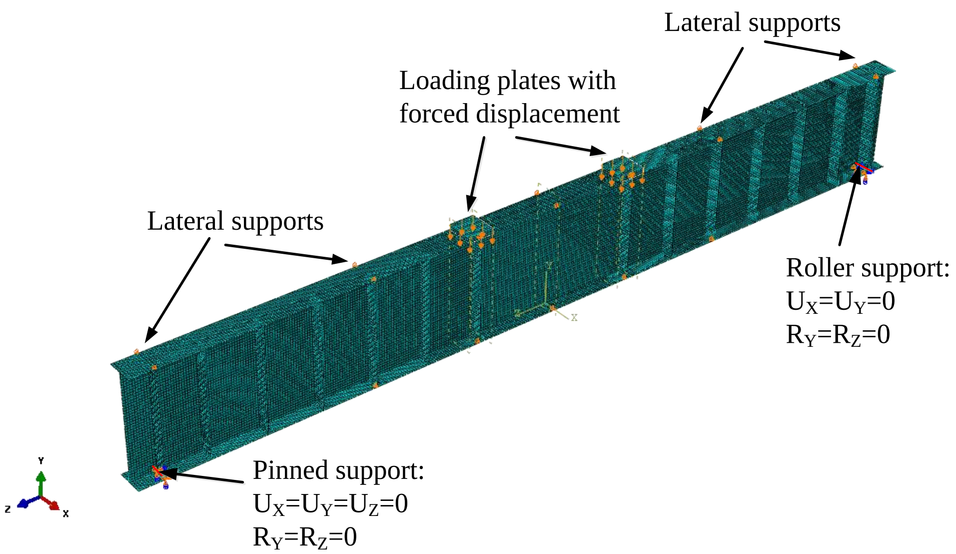

(a) Full span model

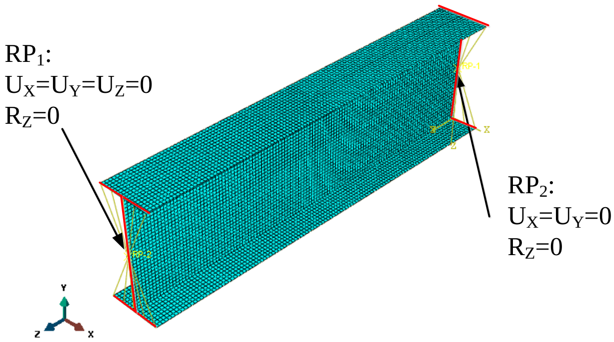

(b) Pure bending model

Fig. 2. Boundary conditions of finite element models

Both initial local geometrical imperfections and residual stresses were also taken into account in the modelling. The local imperfection pattern was obtained by prior eigenvalue buckling analysis under the loading condition. The recommended local buckling imperfection amplitudes e_{EC3} in Eurocode 3 [107] were selected in the parametric study, i.e. b_o /50 is used for I-sections with the flanges as the most critical constituent plate, where b_o is the overhanging width of flange; a/200 is applied for I-sections whose web is more critical than flanges, where a is the minimum flat width of web panel. The typical local imperfection shapes of full span model and pure bending model are presented in **Figs. 3(a) and (b)**, respectively. The unified residual stress pattern proposed by Ban et al. [108] for welded HSS I-sections with $f_{y,nom}$ = 460-960 MPa was adopted in this study with main parameter expressions depicted in **Fig. 4**. In this figure, b_f is the overall width of flange; h_w is the height of web; t_f and t_w represent the thickness of flange and web plates, respectively.

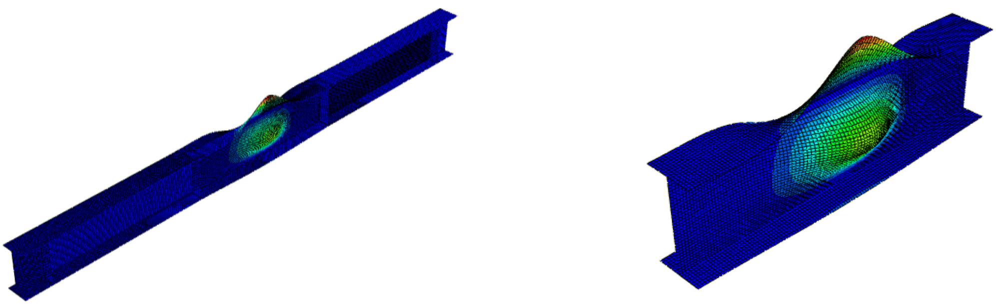

(a) Full span model (b) Pure bending model

Fig. 3. Typical initial local geometrical imperfection shape

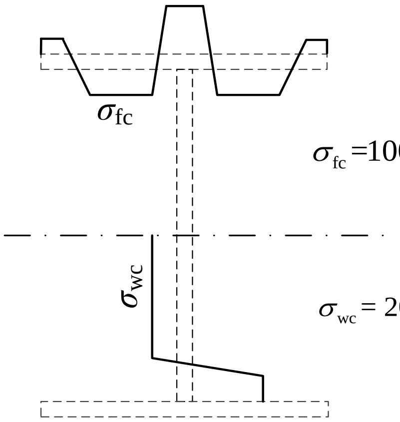

$$\sigma_{fc} = 100 - \frac{930}{b_f / t_f} - \frac{2205}{t_f} \quad -f_y \le \sigma_{fc} < -0.1 f_y$$

$$\sigma_{wc} = 20 - \frac{2200}{h_w / t_w} - \frac{660}{t_w} \quad -f_y \le \sigma_{wc} < -0.1 f_y$$

Fig. 4. Unified residual stress pattern for HSS I-section [108]

3.2 Validation of FE models

The bending test results of square hollow sections, rectangular hollow sections reported by Ma [109], and I-sections reported by Sun et al. [106] were firstly used to validate the effectiveness of the pure bending modelling method. Comparison results of ultimate moment capacities between tests $M_{u,\text{ test}}$ and pure bending models $M_{u,\text{ FE}}$ are given in **Table 7**. The adopted material properties, geometrical and structural initial imperfections were in accordance with the actual values in the literature for the validation.

Table 7 Comparison of ultimate moment capacities between tests and pure bending models based on measured local geometric imperfections

Reference	Specimen	$M_{u,FE}/M_{u,test}$
[109]	H 80 × 80 × 4	1.040
	H 100 × 100 × 4	1.009
	H 120 × 120 × 4	1.015
	H 140 × 140 × 5	1.025
	H 140 × 140 × 6	1.031
	H 160 × 160 × 4	1.052
	H 100 × 50 × 4	0.964
	H 50 × 100 × 4	0.987
	H 200 × 120 × 5	1.012
	H 120 × 200 × 5	0.992
[106]	I-50 × 50 × 5-MA	0.968
	I-70 × 70 × 5-MA	0.955

	I-80 × 60 × 5-MA	0.985
	I-90 × 70 × 5-MA	0.983
	I-100 × 100 × 5-MA	0.985
	I-140 × 70 × 5-MA	0.978
Mean		0.999
CoV		0.028

CoV: Coefficient of Variation

The developed numerical method with the selected local buckling shape and residual stress distribution described in Section 3.1 is further validated against the reported 4-point loading experimental results of HSS I-beams [34,82,93,104,105]. The ratio of maximum flexural strength obtained by finite element analysis $M_{u,\ FE}$ to that from experiments $M_{u,\ test}$ is given in **Table 8**. For comparison, results from full span models, as well as pure bending models with the measured geometrical imperfections are also presented in the table. The statistical results in both **Tables 7 and 8** show that the FE modelling method described in previous section is capable of accurately simulating the ultimate moment capacities of I-sections. The employment of geometric imperfections given in Eurocode 3 also generate the FE results that are in good agreements with test results.

Table 8 Comparison of numerical ultimate moment capacities obtained based on local geometric imperfection magnitudes in Eurocode 3 with experimental results

Reference	Specimen	$M_{u,FE}/M_{u,test}$			
		Full span model with loading plate		Pure bending model	
		Measured imperfection	e_{EC3}	Measured imperfection	e_{EC3}
[104]	7	/	1.007	/	0.988
	8	/	1.005	/	0.991
[105]	HSB800-NC-LP-4-A	/	0.945	/	0.961
[34]	C1	0.996	0.980	0.994	0.993
	C3	1.017	1.017	1.016	1.016
[82]	I-690-2	/	1.075	/	1.070
	I-890-2	/	0.996	/	0.995

[93]	Y11-4	0.997	0.996	0.996	0.998
	Y12-4	0.943	0.942	0.930	0.928
	Y15-4	0.947	0.960	0.946	0.947
	Mean	0.980	0.992	0.976	0.989
	CoV	0.031	0.037	0.034	0.037

CoV: Coefficient of Variation

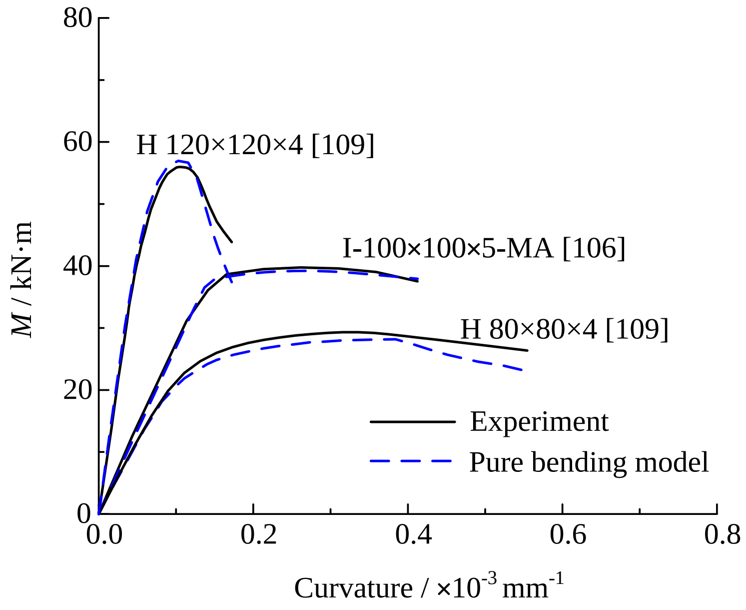

Fig. 5. Comparison of normalized test curves and numerical moment-rotation curves obtained by pure bending modelling for HSS beams with different cross-sections

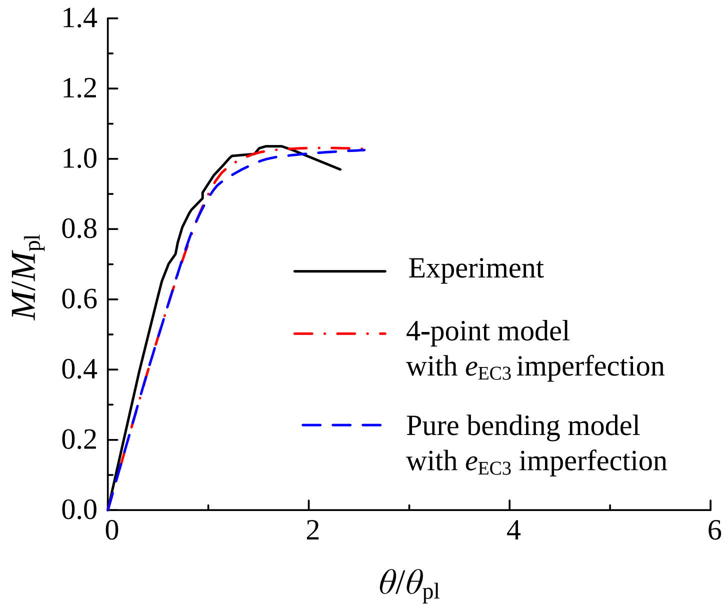

(a) Specimen Y11-4 [93]

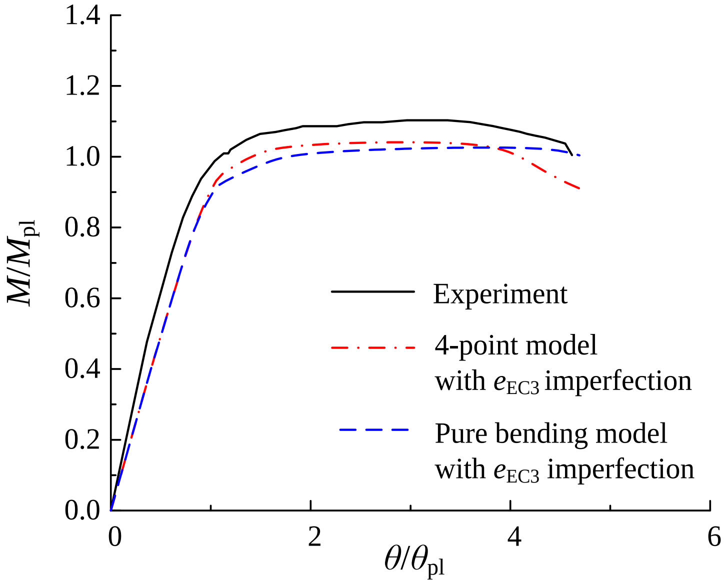

(b) Specimen Y12-4 [93]

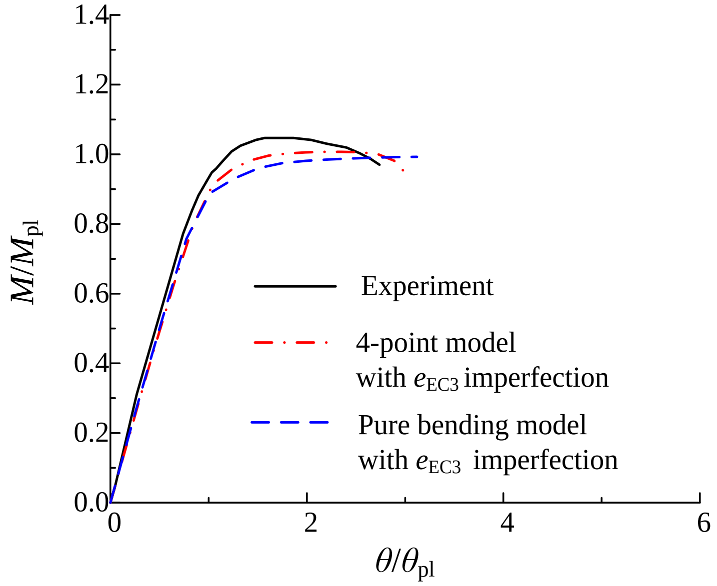

(c) Specimen Y15-4 [93]

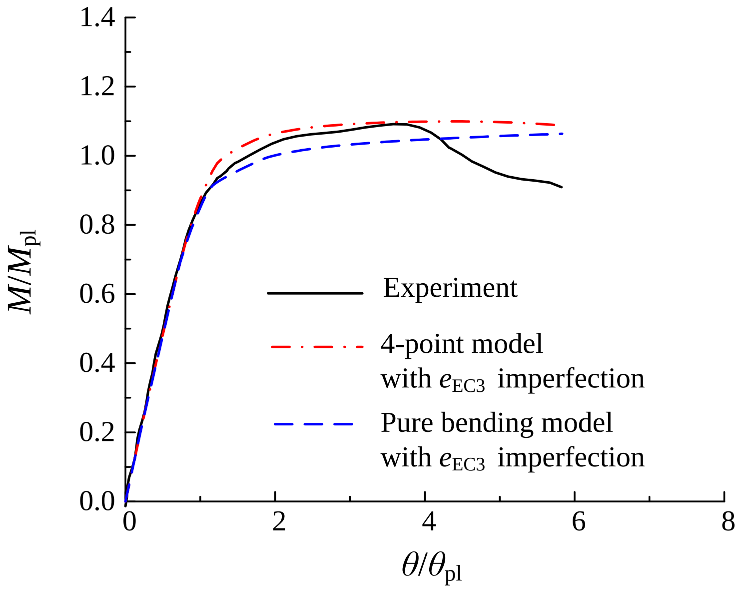

(d) Specimen 7 [104]

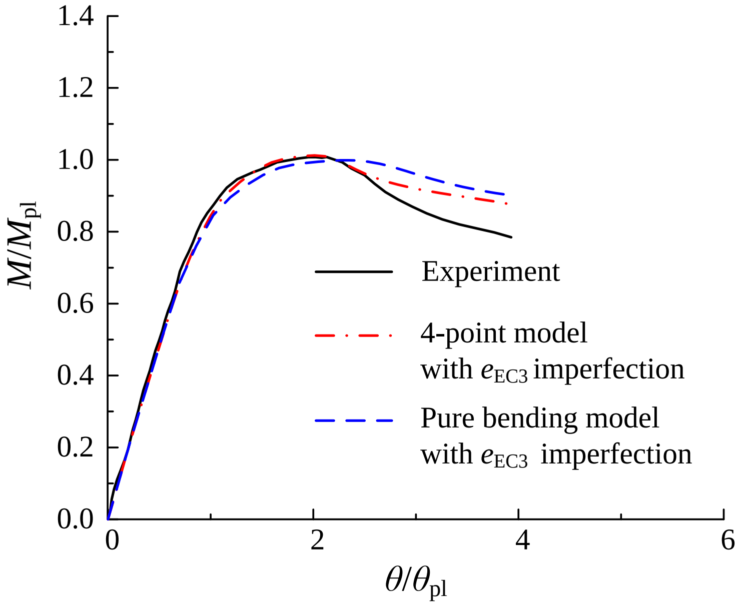

(e) Specimen 8 [104]

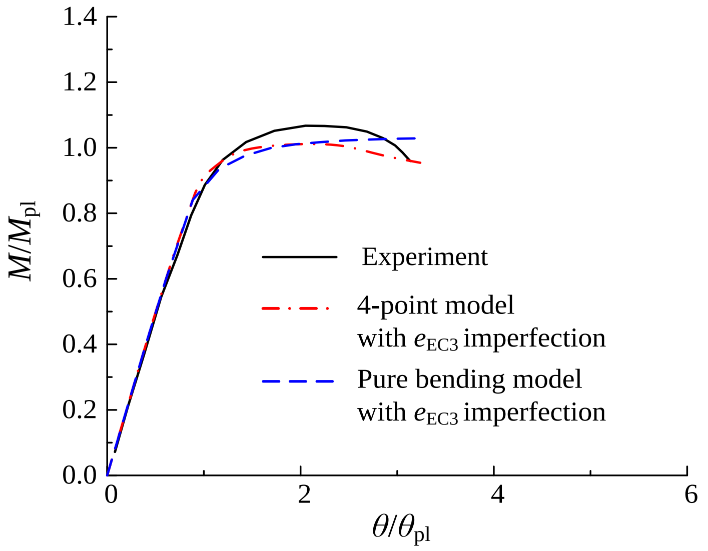

(f) HSB800-NC-LP-4-A [105]

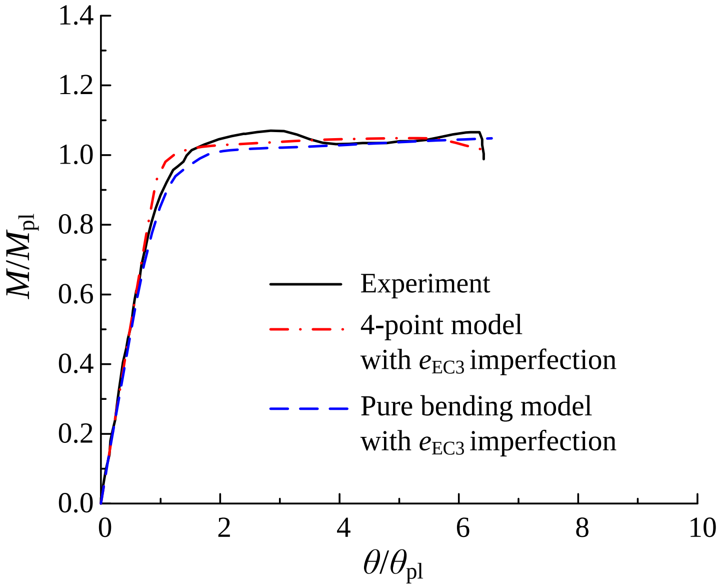

(g) C1 [34]

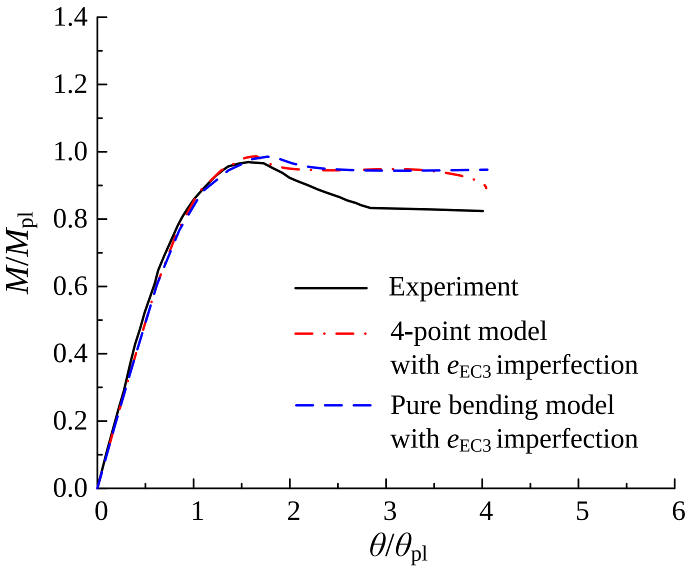

(h) C3 [34]

Fig. 6. Comparison of normalized test curves and numerical moment-rotation curves using adopted finite element methods for HSS I-beams

Furthermore, **Figs. 5** and **6** show the comparisons of normalized moment-rotation responses obtained in experiments and numerical modelling. Generally, the FE models are able to capture the local buckling behaviour of flexural members. Besides, **Fig. 7** displays the consistency between the reported failure mode in the literature and the simulation results in this study. Based on all the above results, it can be concluded that the local buckling behaviour of I-beams could be accurately simulated by pure bending model with the local imperfection amplitude recommended by Eurocode 3 [107] and the adopted residual stress distribution pattern [108].

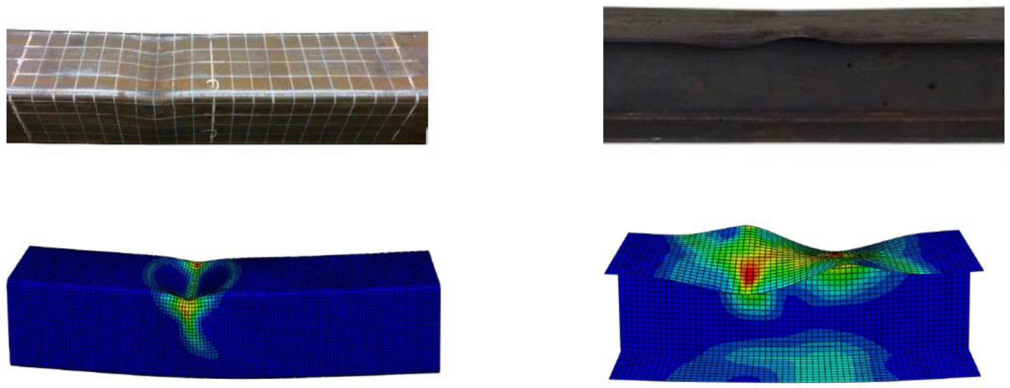

(a) H 140 × 140 × 5 [109]   (b) I-100 × 100 × 5-MA [106]

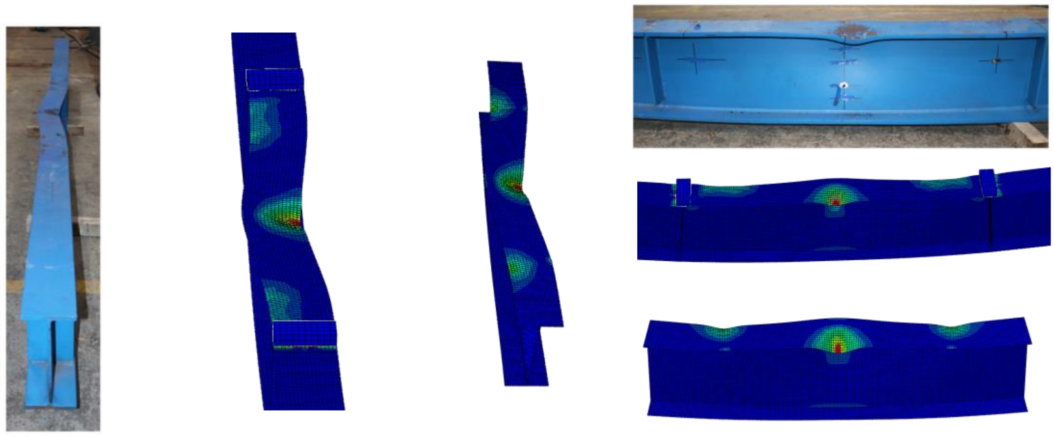

(c) Y15-4 [93]

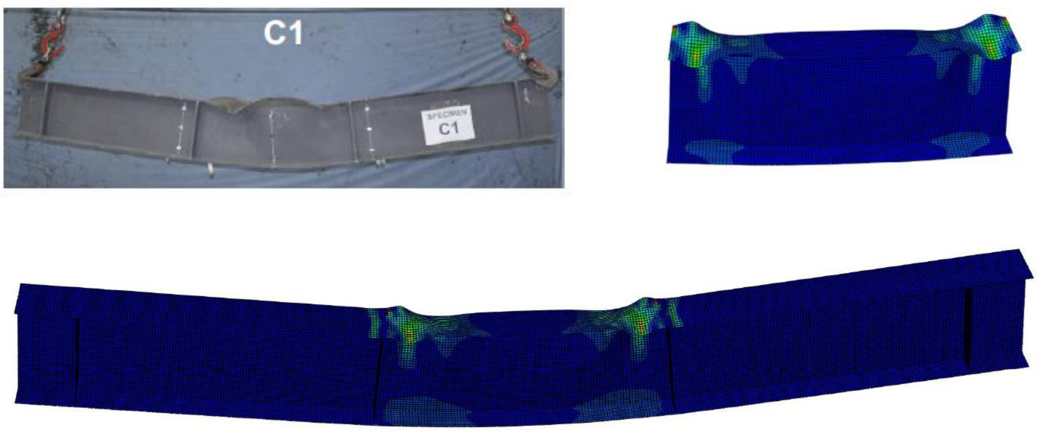

(d) C1 [34]

Fig. 7. Comparison of experimental and numerical failure modes

3.3 Parametric study

Upon the validation of the FE model, parametric studies on HSS I section under bending were conducted. The true stress-strain curves transformed from the average measured steel stresses f_y and f_u of the collected HSS material properties were employed in the numerical simulation for parametric studies. The HSSs with $f_{y,nom}$ = 460 MPa and $f_{y,nom}$ = 690-700 MPa were considered in the parametric study, since most of the available material test data presented in Section 2.1 were generated for these HSS materials, as presented in **Table 5**. The elastic modulus E was taken as 210 GPa [107]. The values of strains ε_u and ε_{sh} were determined based on the stress-strain data of HSS materials (see Eqs. **(9)** and **(10)**). All the above material characteristics are summarized in **Table 9**. The multi-linear constitutive model shown in **Fig. 1(b)** was applied to describe the steel stress-strain relationship in the parameter study.

Table 9 Material properties employed in the parametric study

$f_{y,nom}$ /MPa	f_y /MPa	f_u /MPa	f_y / f_u	ε_{sh} (%)	ε_u (%)
460	521	637	0.818	2.68	10.9
690-700	766	822	0.933	2.0	6.7

In order to cover a wide range of parameters, the dimension of the studied I-sections is determined by the following principles:

(1) The flange slenderness b_f/t_f: 4, 6, 8, 10, 12, 14, 16, 18, 20, 22, 24, 26, 28;

(2) The web slenderness h_w/t_w: 20, 30, 40, 50, 60, 70, 80, 90, 100, 110, 120;

(3) The aspect ratio H/t_w: 1-5;

(4) The thickness of flanges t_f and web t_w (unit: mm): t_f =14, t_w= 6; t_f =10, t_w= 6; t_f = 6, t_w= 6;

where, H represents the height of whole section. Only double-symmetric I-sections were investigated in this study. In the above principles, the ranges of flange and web slenderness were selected to ensure that all the classes of constituent plate elements in European and American codes were covered, and the aspect ratios were selected to cover the universal section sizes of I-beams by referring to those of hot-rolled sections [110]. For I-sections, similar overall cross section slenderness may be achieved by the local buckling of different dominant element plates, as illustrated by **Fig. 8**, so the three combinations of plate thickness were examined. In this figure, $\sigma_{cr,f}$ and $\sigma_{cr,w}$ are the elastic buckling stresses of flange and web plates, respectively.

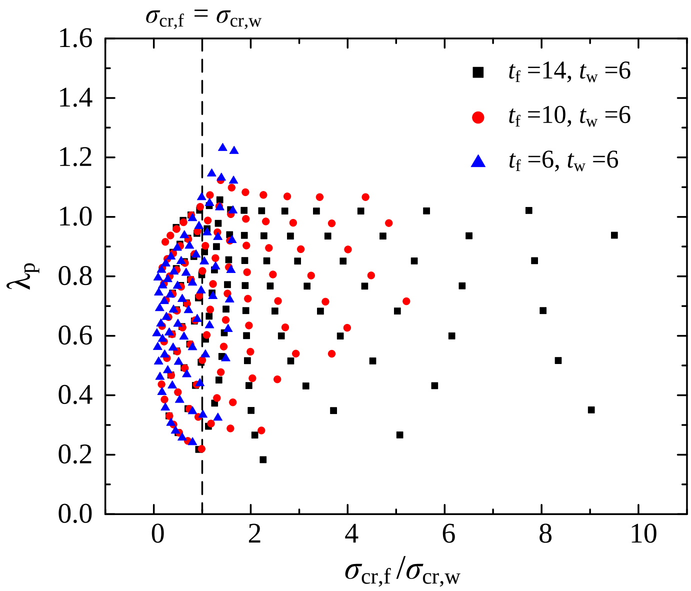

Fig. 8. Relation between overall cross section slenderness and the elastic buckling stress ratio of flange to web

A total of 526 FE models with λ_p = 0.18-1.5 were analysed with the elastic critical moment M_{cr} determined using the eigenvalue buckling analysis in Abaqus. The length l of models was selected to be $4h_w$ for the calculation of elastic buckling stress M_{cr}, whilst $2h_w$ was selected for ultimate moment capacity M_u. This selection principle is illustrated by **Fig. 9** where the results for M_{cr}, M_u of steels with $f_{y,nom}$ = 460 MPa and $f_{y,nom}$ = 690-700 MPa from two representative I-sections are presented. The selected lengths for M_{cr} and M_u were taken as benchmarks, and represented by M_0 in these figures. **Fig. 9(a)** is from the I-section governed by flange local buckling, while the local buckling half-wave of the section shown by **Fig. 9(b)** is mainly affected by web. Despite a member length of at least 3 times the width of the widest plate element is recommended for sections governed by local buckling, the results in **Fig. 9** indicated that l = $2h_w$ is feasible for ultimate moment capacity calculation because of the presence of geometrical and material imperfections. In addition, sufficient lateral restraints were provided so that local buckling of the HSS I-sections under bending is the focus for the parametric studies.

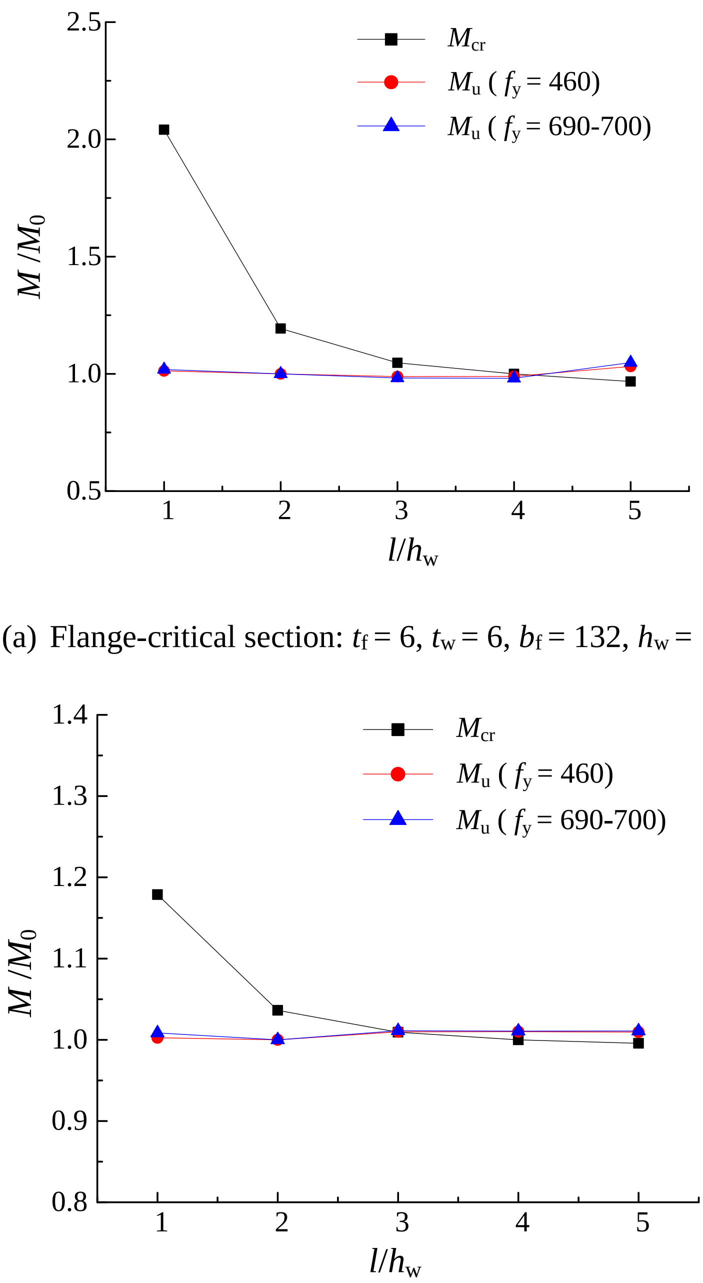

(a) Flange-critical section: $t_f = 6$, $t_w = 6$, $b_f = 132$, $h_w = 120$

(b) Web-critical section: $t_f = 14$, $t_w = 6$, $b_f = 168$, $h_w = 660$

Fig. 9. Effect of member length on the simulation results (unit: mm)

Numerical results of ultimate moment capacity M_u normalized by full plastic moment M_{pl} against the overall cross-section slenderness λ_p are shown in **Fig. 10**. It was observed that limiting slenderness $\lambda_p = 0.51$ can be applied to distinguish different levels of stress distribution for HSS I-section under bending. In other words, the cross-sections with λ_p less than 0.51 are able to develop M_{pl}, whereas section with λ_p higher than 0.51 cannot achieve plastic moment which primarily attribute to the occurrence of local buckling. This limit value is consistent with the results from [19] for hot-rolled steel cross-sections with $\lambda_p = 0.15$-0.68. Furthermore, **Fig.**

11 displays FE results of ultimate moment capacity M_u normalized by M_{el} against the overall cross section slenderness λ_p, where λ_p = 0.776 was found to be the appropriate limiting slenderness classifying slender and non-slender I-sections, which is in line with the observations from [23] for HSS square and rectangular hollow sections in bending.

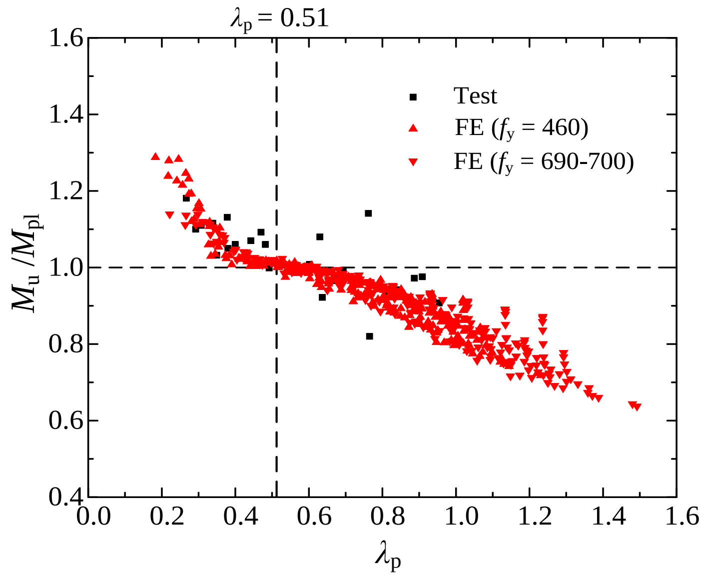

Fig. 10. Ultimate moment capacity M_u normalized by plastic moment capacity M_{pl} of HSS I-section models

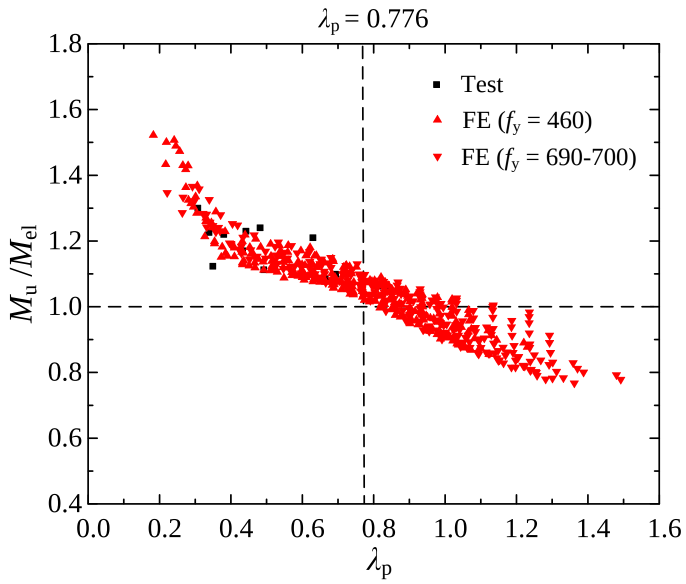

Fig. 11. Ultimate moment capacity M_u normalized by elastic moment capacity M_{el} of HSS I-sections

4 Design methods for local buckling behaviour of HSS I-sections in bending

Based on the generated parametric studies results combined with collected experimental results in literature, the applicability of continuous strength method, direct strength method and Kato's method to HSS I-section under bending was evaluated in this section. Modifications to the methods for more accurate strength predictions were also proposed.

4.1 Continuous strength method

The CSM is a deformation-based design approach firstly proposed by Gardner and Nethercot [111] for the design of stainless steel members considering their local-buckling resistance. The two main components of the CSM are: base curve and material model. The base curve describes the continuous relation between the slenderness of overall cross-section λ_p and its deformation capacity, which is taken as the ratio of ε_{CSM} to ε_y. Here, ε_{CSM} is defined as the limiting strain level of cross-section before failure. An appropriate material model of the CSM is also indispensable to transform section bearing capacity from the deformation-level to strength-level for design resistance calculation. The CSM base curve and material model for HSS I-sections in bending are discussed in details in the following subsections.

4.1.1 Base curve

The CSM base curve describes the relation between the deformation capacity $\varepsilon_{CSM}/\varepsilon_y$ and the overall slenderness of cross-sections λ_p. For the materials with a distinct yield plateau, the deformation capacity $\varepsilon_{CSM}/\varepsilon_y$ of bending members can be calculated by [112,113]

$$\frac{\varepsilon_{CSM}}{\varepsilon_y} = \frac{\kappa_u y_{max}}{\kappa_{el} y_{max}} \text{ for non-slender section} \tag{2}$$

$$\frac{\varepsilon_{CSM}}{\varepsilon_y} = \frac{M_u}{M_{el}} \text{ for slender section} \tag{3}$$

where, κ_u and κ_{el} represent the curvatures of members at M_u and M_{el}, respectively; y_{max} is the distance between the elastic neutral axis and the extreme fibre of sections.

As mentioned in Section 3.3, the relation between M_u/M_{el} and λ_p observed in this study is consistent with that in [23], so the base curve established by Lan et al., whose expressions are indicated by Eqs. **(4)** and **(5)**, were firstly evaluated. In Eq. **(4)**, C_1 is the coefficient used to avoid over-strength predictions. The assessed results are given in **Fig. 12**, it can be seen that the base curve provides the reasonable prediction results for HSS I-sections in bending. For consistent application of the CSM to structures with different cross-section shapes under bending, the base curve from [23] is adopted and used in this study with the coefficients introduced in the previous Section 3.1.

$$\frac{\varepsilon_{\mathrm{CSM}}}{\varepsilon_{\mathrm{y}}}=\frac{0.50}{\lambda_{\mathrm{p}}^{2.74}}\leq\min\left(15,\frac{C_1\varepsilon_{\mathrm{u}}}{\varepsilon_{\mathrm{y}}}\right)\ \text{for}\ 0.15<\lambda_{\mathrm{p}}\leq0.776 \tag{4}$$

$$\frac{\varepsilon_{\mathrm{CSM}}}{\varepsilon_{\mathrm{y}}}=\left(1-\frac{0.10}{\lambda_{\mathrm{p}}^{0.47}}\right)\frac{1}{\lambda_{\mathrm{p}}^{0.47}}\ \text{for}\ 0.776<\lambda_{\mathrm{p}}\leq1.5 \tag{5}$$

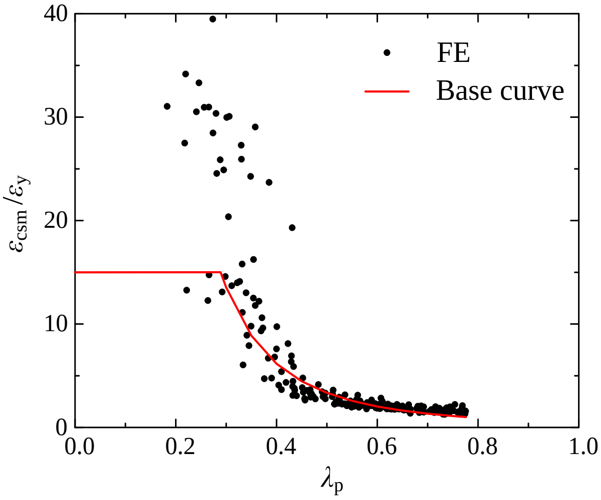

(a) $\lambda_{\mathrm{p}}\leq0.776$

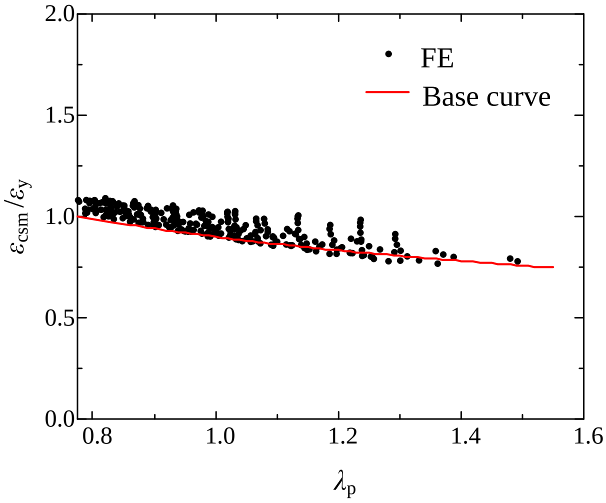

(b) $\lambda_{\mathrm{p}}>0.776$

Fig. 12. Assessment of the base curve proposed by Lan et al. [23] for HSS I-sections in bending

4.1.2 Material model

A quad-linear stress-strain CSM model, as depicted in **Fig. 13**, has been proposed by Yun and Gardner [114] for hot-rolled steel. In this figure, E_{sh} is strain hardening modulus; C_2 is the model coefficient used to determine E_{sh}. The expressions of the ultimate strain ε_u, the strain at onset of strain hardening ε_{sh} and the model coefficients (C_1 and C_2) for hot-rolled steel are given by Eqs. **(6)-(8)**.

$$\varepsilon_u = 0.6\left(1-\frac{f_y}{f_u}\right), \quad \text{and } \varepsilon_u \geq 0.06 \tag{6}$$

$$\varepsilon_{sh} = 0.1\frac{f_y}{f_u} - 0.055, \quad \text{and } 0.015 \leq \varepsilon_{sh} \leq 0.03 \tag{7}$$

$$C_1 = \frac{\varepsilon_{sh} + 0.25\left(\varepsilon_u - \varepsilon_{sh}\right)}{\varepsilon_u}; \quad C_2 = \frac{\varepsilon_{sh} + 0.4\left(\varepsilon_u - \varepsilon_{sh}\right)}{\varepsilon_u} \tag{8}$$

In **Tables 2-4**, the references included in Yun and Gardner's database are highlighted by "△". It is clear that they only occupy a rather small fraction of HSS database established in this study. For this end, a modification of the aforementioned expressions for ε_u, ε_{sh}, C_1 and C_2 in the quad-linear material model is required to establish the CSM material model for HSS, as illustrated in the subsequent sections.

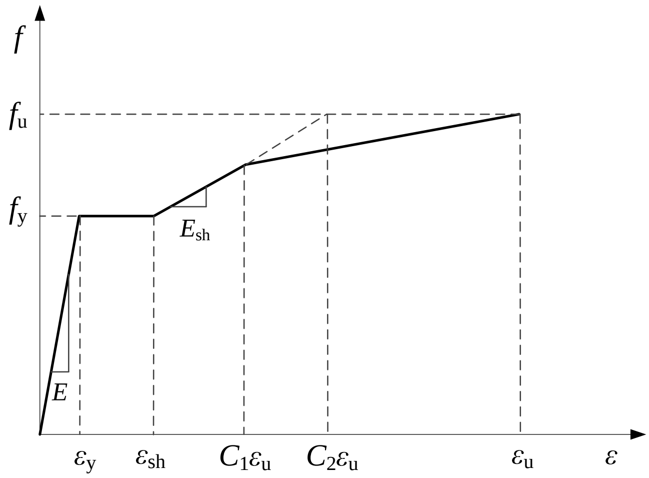

Fig. 13. The quad-linear material model for hot-rolled steels by Yun and Gardner [114]

4.1.2.1 Ultimate strain ε_u

In Eurocode 3 [115], f_u/f_y of steel is recommended to be greater than 1.05 for HSS, therefore the material test results failed to meet this requirement were excluded. The relation between ε_u and f_y/f_u for HSS covering various spectrums of steel grade was proposed as depicted by **Fig. 14** and Eq. **(9)** based on regression analysis. In **Fig. 14**, "■", "●" and "◆" represent that f_y/f_u of the tested materials belong to "$0.9 < f_y/f_u$", "$0.85 < f_y/f_u \leq 0.9$" and "$f_y/f_u \leq 0.85$", respectively.

In particular, the prediction expression for the steel with $f_y/f_u \leq 0.85$ is consistent with that proposed for hot-rolled steel by Yun and Gardner [114].

$$\varepsilon_u = \begin{cases} 0.6\left(1-\dfrac{f_y}{f_u}\right) & f_y/f_u \leq 0.85 \\ 0.8\left(1-\dfrac{f_y}{f_u}\right) & 0.85 < f_y/f_u \leq 0.9 \\ 1-\dfrac{f_y}{f_u} & 0.9 < f_y/f_u \end{cases} \tag{9}$$

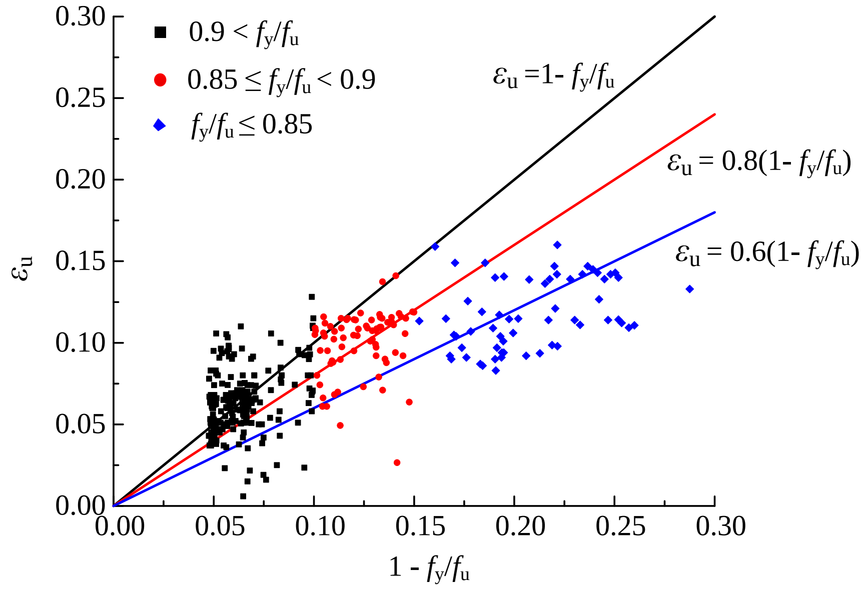

Fig. 14. Relation between ultimate strain and yield-to-tensile ratio

4.1.2.2 Strain ε_{sh} at onset of strain hardening

Different from ε_u, the values of strain at onset of strain hardening ε_{sh} may not be always given in the literature. Therefore, most of test data of ε_{sh} in this study, which is presented in **Fig. 15**, are extracted from the available full stress-strain curves. In Yun and Gardner's study [114], ε_{sh} was given by a constant value 0.03 for steels with $0.85 \leqslant f_y/f_u$ probably due to the limited and scattered data points in this zone. In this study, more precise prediction expressions for ε_{sh} in "$0.85 < f_y/f_u \leq 0.9$"and "$0.9 < f_y/f_u$" subdivisions were generated through regression analysis using the established data and are given as Eq. **(10)**, while the relation between ε_{sh} and f_y/f_u in the "$f_y/f_u \leq 0.85$" zone follows the equation from Yun and Gardner [114]. The data shown in **Fig. 15** are based on the curves with distinct yield plateau. Although the yield plateau may not be observed for the HSS with relatively higher f_y, Eq. **(10)** is considered to be acceptable for all the HSS materials except for those with $f_{y,nom} \geq 890$ MPa, as it would provide conservative strength predictions for those $f_{y,nom}$ = 500-700 MPa steel without a yield plateau. For HSS with $f_{y,nom}$ = 890-1100 MPa, ε_{sh} can be simply taken as 0.

$$\varepsilon_{sh}=\begin{cases}0.1\dfrac{f_y}{f_u}\text{-}0.055 & f_y/f_u \le 0.85\\ -0.2\dfrac{f_y}{f_u}+0.2 & 0.85 < f_y/f_u \le 0.9\\ 0.02 & 0.9 < f_y/f_u\end{cases} \tag{10}$$

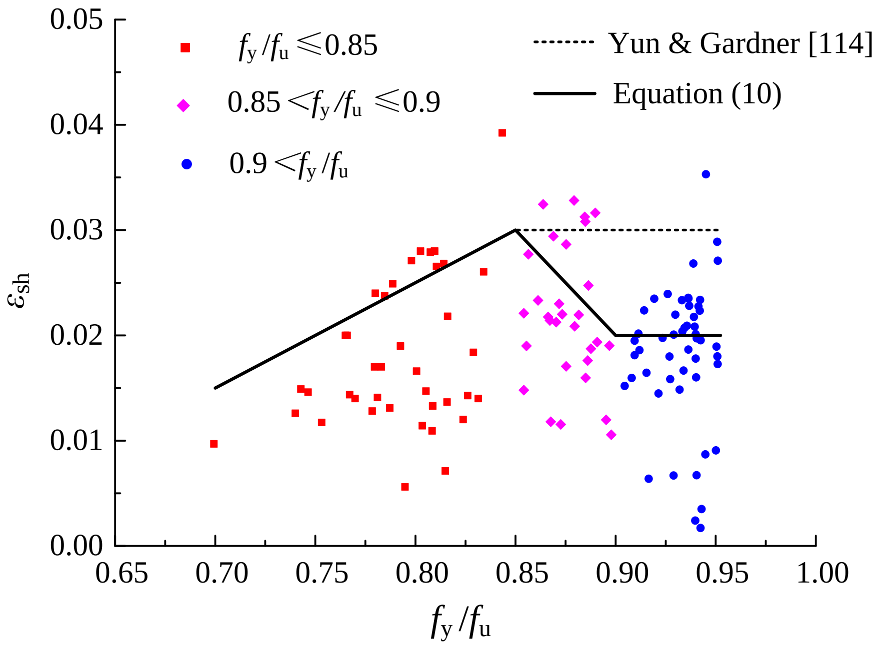

Fig. 15. Relation between strain hardening strain and yield-to-tensile ratio

4.1.2.3 Model coefficients

A total of 190 full measured stress-strain curves of HSS were collected and used to obtain the material strain hardening characteristics to determine the coefficients C_1 and C_2 for the CSM material model. Due to the unevenly distributed data points of test curves, each curve was firstly fitted with 7-order polynomial [116]. Subsequently, the portion above yield plateau regions of each fitted curve was depicted in normalised form to describe the strain hardening properties for HSS. Based on a series of data analysis, expressions for estimating the coefficients C_1 and C_2 of HSS materials were obtained as Eqs. **(11)** and **(12)**, which are on the conservative side for ninety percent of strain-hardening curves in database. All the normalised stress-strain curves are shown in **Fig. 16** with the proposed CSM material model in the strain hardening region. For comparison purposes, the model from Yun and Gardner [114] is also presented in this figure and shown to provide overestimation for the strain-hardening of HSS materials. **Table 10** summarizes the predictive expressions below as the CSM material model for HSS.

$$C_1 = \frac{\varepsilon_{\mathrm{sh}} + 0.3\left(\varepsilon_{\mathrm{u}} - \varepsilon_{\mathrm{sh}}\right)}{\varepsilon_{\mathrm{u}}} \tag{11}$$

$$C_2 = \frac{\varepsilon_{\mathrm{sh}} + 0.55\left(\varepsilon_{\mathrm{u}} - \varepsilon_{\mathrm{sh}}\right)}{\varepsilon_{\mathrm{u}}} \tag{12}$$

$$E_{\mathrm{sh}} = \frac{f_{\mathrm{u}} - f_{\mathrm{y}}}{0.55\left(\varepsilon_{\mathrm{u}} - \varepsilon_{\mathrm{sh}}\right)} \tag{13}$$

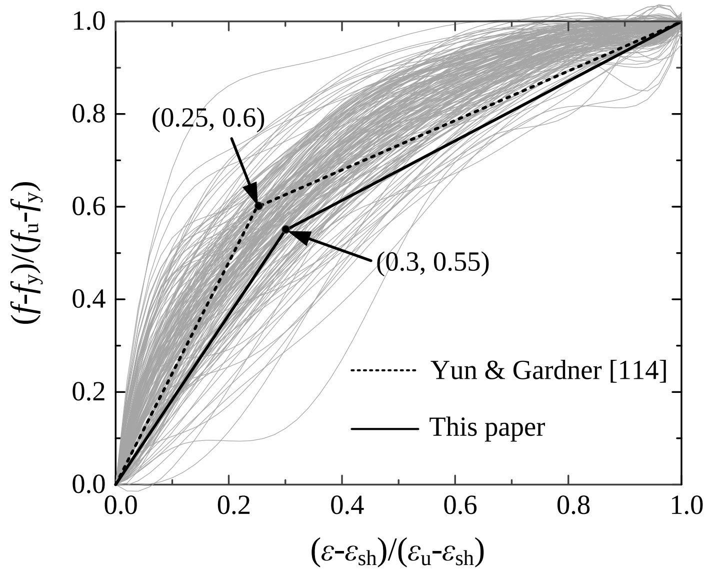

Fig. 16. Comparison of the reported stress-strain curves and the proposed CSM material model for HSS in the strain hardening region

Table 10 The CSM material model for HSS materials

<table>
<tr><th></th><th>ε_{u}</th><th>$\varepsilon_{\mathrm{sh}}$</th><th>$C_1$</th><th>$C_2$</th></tr>
<tr><td>$f_{\mathrm{y}}/f_{\mathrm{u}} \leq 0.85$</td><td>$0.6\left(1-\frac{f_{\mathrm{y}}}{f_{\mathrm{u}}}\right)$</td><td>$0.1\frac{f_{\mathrm{y}}}{f_{\mathrm{u}}}-0.055$</td><td rowspan="3">$\frac{\varepsilon_{\mathrm{sh}}+0.3\left(\varepsilon_{\mathrm{u}}-\varepsilon_{\mathrm{sh}}\right)}{\varepsilon_{\mathrm{u}}}$</td><td rowspan="3">$\frac{\varepsilon_{\mathrm{sh}}+0.55\left(\varepsilon_{\mathrm{u}}-\varepsilon_{\mathrm{sh}}\right)}{\varepsilon_{\mathrm{u}}}$</td></tr>
<tr><td>$0.85 < f_{\mathrm{y}}/f_{\mathrm{u}} \leq 0.9$</td><td>$0.8\left(1-\frac{f_{\mathrm{y}}}{f_{\mathrm{u}}}\right)$</td><td>$-0.2\frac{f_{\mathrm{y}}}{f_{\mathrm{u}}}+0.2$</td></tr>
<tr><td>$0.9 < f_{\mathrm{y}}/f_{\mathrm{u}}$</td><td>$1-\frac{f_{\mathrm{y}}}{f_{\mathrm{u}}}$</td><td>0.02</td></tr>
<tr><td colspan="5">Note: for the steel with $f_{\mathrm{y,nom}} \geq 890$ MPa, $\varepsilon_{\mathrm{sh}}$ can be simply taken as 0.</td></tr>
</table>

4.1.3 Cross-section resistance

For steel materials with a well-defined yield point, the expression of CSM material stress f_{CSM} and cross-section resistance M_{CSM} have been provided by Yun and Gardner [19,114], which are expressed by Eqs. **(14)** and **(15)**.

$$f_{\mathrm{CSM}} = \begin{cases} E\varepsilon_{\mathrm{CSM}} & \text{for } \varepsilon_{\mathrm{CSM}} \le \varepsilon_{\mathrm{y}} \\ f_{\mathrm{y}} & \text{for } \varepsilon_{\mathrm{y}} < \varepsilon_{\mathrm{CSM}} \le \varepsilon_{\mathrm{sh}} \\ f_{\mathrm{y}} + E_{\mathrm{sh}}\left(\varepsilon_{\mathrm{CSM}} - \varepsilon_{\mathrm{sh}}\right) & \text{for } \varepsilon_{\mathrm{sh}} < \varepsilon_{\mathrm{CSM}} \le C_1\varepsilon_{\mathrm{u}} \end{cases} \tag{14}$$

and

$$M_{\mathrm{CSM}} = \begin{cases} \dfrac{\varepsilon_{\mathrm{CSM}}}{\varepsilon_{\mathrm{y}}} M_{\mathrm{el}} & \text{for } \varepsilon_{\mathrm{CSM}} \le \varepsilon_{\mathrm{y}} \\ M_{\mathrm{pl}}\left[1 - \left(1 - \dfrac{W_{\mathrm{el}}}{W_{\mathrm{pl}}}\right) \Big/ \left(\dfrac{\varepsilon_{\mathrm{CSM}}}{\varepsilon_{\mathrm{y}}}\right)^{\alpha}\right] & \text{for } \varepsilon_{\mathrm{y}} < \varepsilon_{\mathrm{CSM}} \le \varepsilon_{\mathrm{sh}} \\ M_{\mathrm{pl}}\left[1 - \left(1 - \dfrac{W_{\mathrm{el}}}{W_{\mathrm{pl}}}\right) \Big/ \left(\dfrac{\varepsilon_{\mathrm{CSM}}}{\varepsilon_{\mathrm{y}}}\right)^{\alpha} + \beta\left(\dfrac{\varepsilon_{\mathrm{CSM}} - \varepsilon_{\mathrm{sh}}}{\varepsilon_{\mathrm{y}}}\right)^{2} \dfrac{E_{\mathrm{sh}}}{E}\right] & \text{for } \varepsilon_{\mathrm{sh}} < \varepsilon_{\mathrm{CSM}} \le C_1\varepsilon_{\mathrm{u}} \end{cases} \tag{15}$$

In Eq. **(15)**, α and β are the coefficients introduced to give approximate estimations of the lengthy theoretical expressions for cross-section resistance calculation. The values of α and β for I-sections under major-axis bending are selected to be 2 and 0.1 respectively, which have been proven to produce acceptable accuracy for strength predictions [19, 23]. Once the CSM material model for HSS is determined, the cross-section resistance of HSS I-sections in bending could be obtained subsequently by Eqs. **(14)** and **(15)**.

Table 11 Comparison of experimental results and prediction results of design methods

Reference	Specimen	$M_{\mathrm{u,test}}/M_{\mathrm{EC3}}$	$M_{\mathrm{u,test}}/M_{\mathrm{AISC}}$	$M_{\mathrm{u,test}}/M_{\mathrm{CSM}}$	$M_{\mathrm{u,test}}/M_{\mathrm{DSM\text{-}AISI}}$	$M_{\mathrm{u,test}}/M_{\mathrm{DSM,mod}}$	$M_{\mathrm{u,test}}/M_{\mathrm{Kato}}$
[56]	1	1.123	1.039	1.002	1.071	1.032	1.011
	2	1.272	1.125	1.064	1.161	1.116	1.200
	3	1.126	0.994	1.045	1.086	1.037	1.075
	4	1.123	1.074	1.083	1.094	1.086	1.109
	5	1.112	1.006	1.007	1.068	0.999	0.985
	6	1.111	0.944	1.087	1.106	1.093	1.123
	7	1.118	0.975	1.011	1.066	1.005	1.042
[11]	NN-B1	1.246	0.920	1.231	1.244	1.220	1.055
	SS-B2	1.130	1.201	1.076	1.127	1.096	0.987

	NS-B3	1.127	1.130	1.147	1.188	1.162	1.009
	SN-B4	1.172	1.223	1.111	1.144	1.123	1.040
[106]	50×50×5-MA	1.110	1.107	1.064	1.178	1.110	1.105
	70×70×5-MA	1.020	1.034	1.025	1.099	1.020	1.057
	80×60×5-MA	1.050	1.055	1.051	1.127	1.050	1.190
	90×70×5-MA	1.070	1.084	1.076	1.156	1.070	1.050
	100×100×5-MA	1.252	1.228	1.117	1.183	1.111	1.088
	140×70×5-MA	1.060	1.073	1.071	1.165	1.060	1.054
[82]	I-690-2	1.027	0.970	0.954	1.007	0.949	0.919
	I-890-2	1.114	1.059	1.035	1.094	1.027	1.016
Mean		1.12	1.07	1.07	1.12	1.07	1.06
CoV		0.063	0.083	0.059	0.050	0.057	0.065

CoV: Coefficient of Variation

The statistical evaluation results shown in **Table 11** presents the mean ratios of the $M_{u,test}$ as the test results over the strength predictions from the CSM (M_{CSM}). Predictions obtained using Eurocode 3 (M_{EC3}) and AISC Specification (M_{AISC}) are also presented in the table for comparison. It can be seen from this table that all the three approaches provide the conservative predictions on average for the HSS I-sections under bending. Compared with those predictions based on Eurocode 3 and AISC Specifications, the proposed CSM provides more accurate and less scattered predictions. All the data points generated by the CSM are shown **Fig. 17**, together with those obtained based on codified design methods. In this figure, M_u represents the ultimate cross-section resistance from experiments or numerical simulation; $M_{u,pred}$ means the predictive results obtained by different design methods. As can be seen in the figure, both Eurocode 3 and the CSM provide the overall conservative predictions, while the predictive results of AISC specification are relatively more scattered with some $M_u/M_{u,pred}$ ratios below 1 for over-estimating the structural strength. Note that the methods highlighted by "☆" in the figures are those ones newly developed in this study.

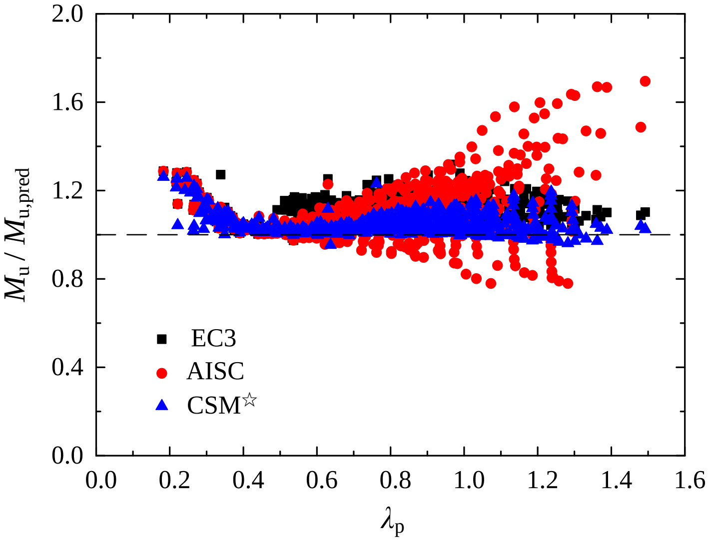

Fig. 17. Comparison of test and FE data with the CSM predictions

4.2 Direct strength method

The DSM is a strength-based method originally developed by Schafer and Pekoz [117] for the cold-formed steel (CFS) sections. It has been specified in the North American and Australian specifications [118] for the design of CFS members with different configurations since the 2000s. For CFS C and Z sections, the current codified DSM formulas considering local buckling is expressed by Eq. **(16)** [21, 117].

$$M_{\text{DSM-AISI}} = \begin{cases} M_{\text{el}} + \left(M_{\text{pl}} - M_{\text{el}}\right)\left(1 - \dfrac{\lambda_{\text{p}}}{0.776}\right) & \text{for } \lambda_{\text{p}} \le 0.776 \\ M_{\text{el}}\left(1 - 0.15\lambda_{\text{p}}^{-0.8}\right)\lambda_{\text{p}}^{-0.8} & \text{for } \lambda_{\text{p}} > 0.776 \end{cases} \quad (16)$$

The comparison results between numerical results of HSS I-beams and the DSM curves generated using Eq. **(16)** are displayed in **Fig. 18**. It is evident that the codified DSM curves greatly underestimate the moment capacity of HSS I-sections in bending, especially for λ_p $\le$0.776. This discrepancy could be attributed to the differences of section properties between those CFS open-sections and HSS I-sections.

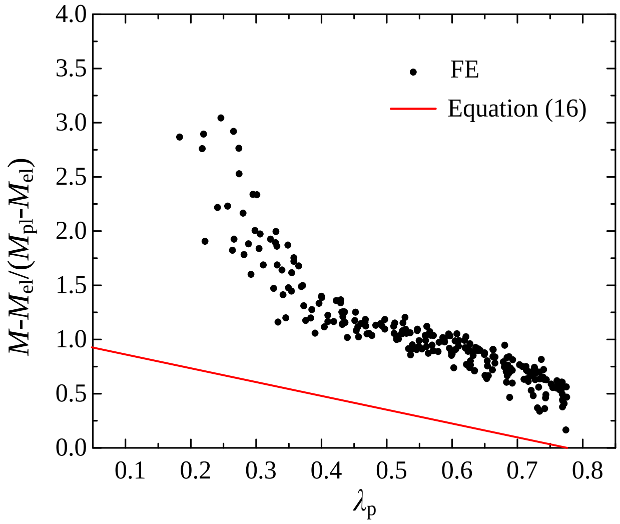

(a) $\lambda_p \leq 0.776$

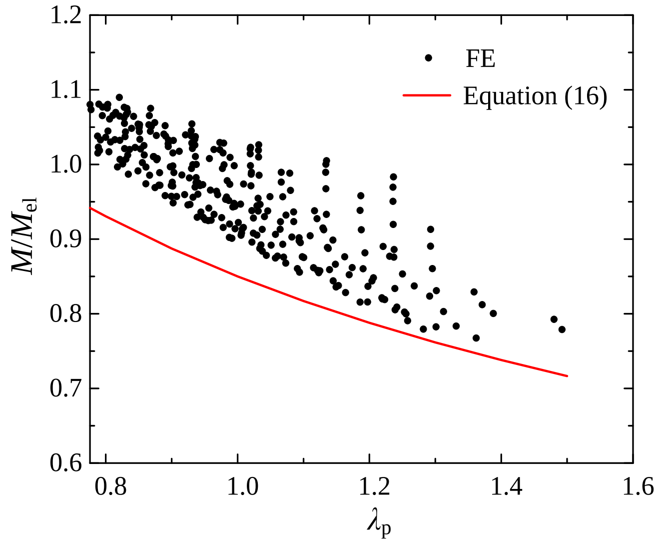

(b) $\lambda_p > 0.776$

Fig. 18. Assessment of the codified DSM curves for HSS I-sections in bending

To extend the DSM for HSS I-sections in bending, a series of regression analysis of FE data was performed by least squares method. The modified DSM expression for HSS I-beams is presented herein as Eq. **(17)**, and the $M_{DSM,mod}$ versus λ_p are plotted in **Fig. 19**. A new subdivision $\lambda_p \leq 0.51$ was established according to the characteristics of moment resistance for I-sections.

$$M_{\mathrm{DSM,mod}} = \begin{cases} M_{\mathrm{pl}} & \text{for } 0.15 < \lambda_{\mathrm{p}} \le 0.51 \\ M_{\mathrm{el}} + 1.7\left(M_{\mathrm{pl}} - M_{\mathrm{el}}\right)\left(1 - \dfrac{\lambda_{\mathrm{p}}}{0.776}\right)^{0.5} & \text{for } 0.51 < \lambda_{\mathrm{p}} \le 0.776 \\ M_{\mathrm{el}}\left(1 - 0.12\lambda_{\mathrm{p}}^{-0.6}\right)\lambda_{\mathrm{p}}^{-0.6} & \text{for } 0.776 < \lambda_{\mathrm{p}} \le 1.5 \end{cases} \tag{17}$$

The predictive accuracy of the codified DSM – Eq. **(16)**, as well as the modified DSM – Eq. **(17)** is shown in **Table 11** in comparison with the results from tests in literature. It can be seen that the modified DSM expression generates more accurate predictions for HSS I-sections subjected to bending in comparison with the original one. **Fig. 20** compares the predictions between the codified and modified DSM by plotting the test (or FE)-to-predicted resistance ratios against λ_{p}, which clearly indicates the improved accuracy of the modified ones.

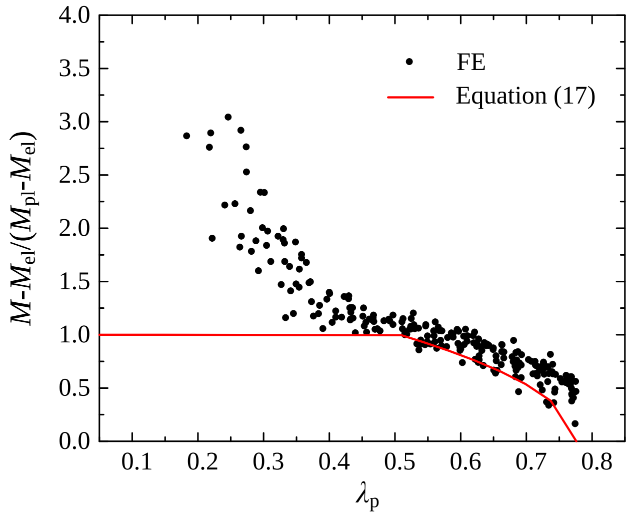

(a) $\lambda_{\mathrm{p}} \le 0.776$

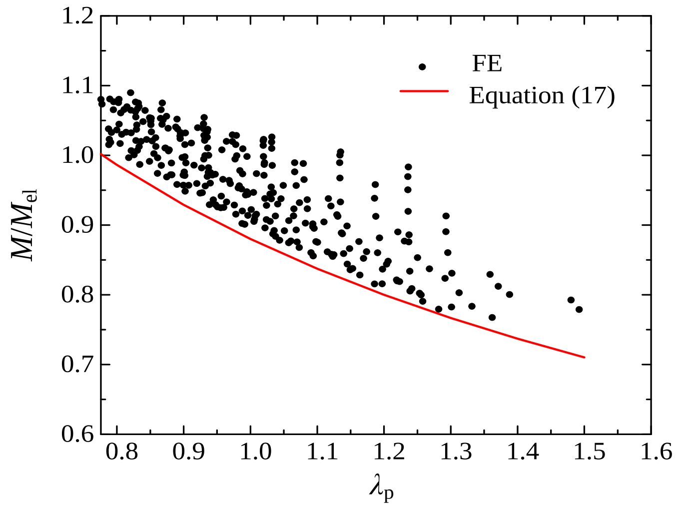

(b) $\lambda_{\mathrm{p}} > 0.776$

Fig. 19. The curves generated by the modified DSM expressions for HSS I-sections in bending

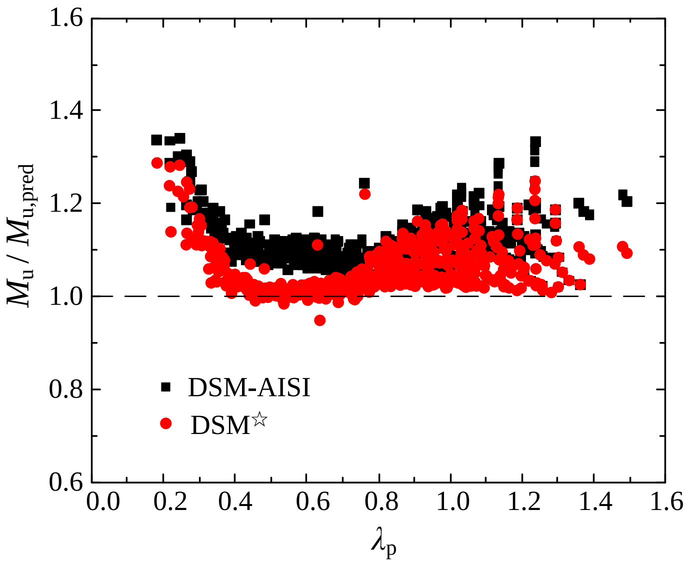

Fig. 20. Comparison of test and FE data with the codified and the modified DSM predictions

4.3 The method from Kato

Kato [25, 26] provided a semi-empirical method to treat the deformation capacity of I-sections failing by local buckling. In this method, based on the assumptions of the rigid-plastic material model and equivalent two-flange geometric model, rotation capacity of members can be derived theoretically as a function of material characteristics, cross-section dimensions as well as the normalized ultimate bearing capacity of members. This normalized ultimate bearing capacity s is defined as the ratio of M_u and M_{el} under the condition of bending. As demonstrated by Eqs. **(18)** and **(19)**, s is calculated using flange slenderness and web slenderness parameters, α_f and α_w, which is an indication of considering the interactive effect of flanges and web.

$$\frac{1}{s}=A+\frac{B}{\alpha_f}+\frac{C}{\alpha_w} \tag{18}$$

where,

$$\alpha_f=\frac{E}{f_{yf}}\left(\frac{t_f}{b_f/2}\right)^2;\ \alpha_w=\frac{E}{f_{yw}}\left(\frac{t_w}{h_w}\right)^2 \tag{19}$$

Where, A, B and C are the material-dependent coefficients, and f_{yf} and f_{yw} are the yield stresses of flanges and web respectively. Underpinned by a regression analysis of established HSS I-beam database in this study, the local buckling resistance M_{Kato} using Kato's method can be expressed by Eq. **(20)**, as illustrated by a smooth surface in **Fig. 21**.

$$\frac{1}{M_{\mathrm{Kato}}/M_{\mathrm{el}}}=0.779+\frac{0.389}{\alpha_{\mathrm{f}}}+\frac{0.005}{\alpha_{\mathrm{w}}} \tag{20}$$

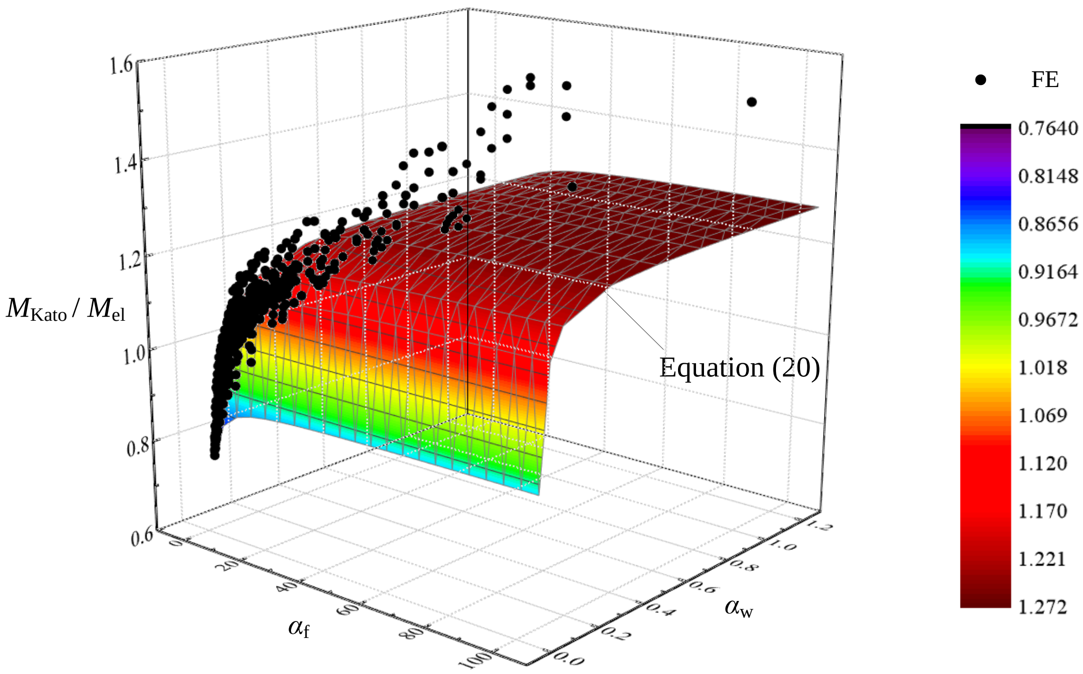

Fig. 21. The surface generated by Kato's method for HSS I-sections in bending

The prediction accuracy of Eq. **(19)** for tests is presented in **Table 11**. A comparison for predictions based on the proposed CSM, the modified DSM and the Kato's method is indicated by **Fig. 22**, with a limiting slenderness λ_{p} = 0.776 classifying non-slender and slender sections. As can be seen from this figure, all the three methods present the similar predictive trend for non-slender sections, namely $\lambda_{\mathrm{p}}<0.776$. For slender sections ($\lambda_{\mathrm{p}}>0.776$) where local buckling is most likely to take place, the predictions from Kato's method show higher accuracy. This might be attributed to the separate consideration for the effect of flange and web slenderness in Kato's expression. By contrast, the overall cross section slenderness-the basis parameter applied in both the CSM and DSM, is unable to identify the buckled plate of I-section, which may lead to the unanticipated prediction error.

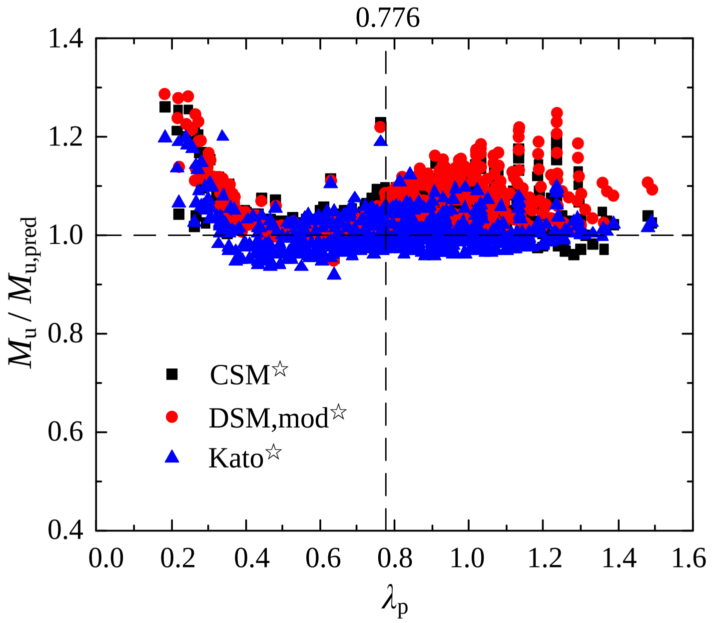

Fig. 22. Comparison of predictive accuracy among the proposed CSM, the modified DSM and the Kato's method

In addition, statistical analysis results for the predictive accuracy of all the design methods against all the test and FE data are shown in **Table 12**. The mean ratios of experimental or numerical results to the predictions from the proposed CSM (M_u/M_{CSM}), the modified DSM ($M_u/M_{DSM,mod}$) and the method from Kato (M_u/M_{Kato}) are 1.05, 1.06 and 1.01, with corresponding CoV of 0.045, 0.051 and 0.041. In comparison, the mean ratios from Eurocode 3 (M_u/M_{EC3}), AISC specification (M_u/M_{AISC}) and the codified DSM ($M_u/M_{DSM\text{-}AISI}$) are greater with more unsatisfactory CoV.

Table 12 Statistical analysis of prediction results for different design methods

	M_u/M_{EC3}	M_u/M_{AISC}	M_u/M_{CSM}	$M_u/M_{DSM\text{-}AISI}$	$M_u/M_{DSM,mod}$	M_u/M_{Kato}
Mean	1.10	1.10	1.05	1.11	1.06	1.01
CoV	0.052	0.125	0.045	0.050	0.051	0.041

CoV: Coefficient of Variation

5 Reliability analysis of design methods

The first-order reliability method specified in Eurocode 3 [28] was used to assess the reliability level of the proposed design expressions in this study. The material over-strength $f_{y,mean}/f_{y,nom}$, determined based on the established HSS database in this study, was selected to be 1.12 with the CoV = 0.066. The CoV of geometric properties was taken as 0.05, referring to the recommended values for the fabrication of stainless and aluminium steels [119,120]. The reliability analysis results were shown in **Table 13**. In this table, b is the average ratio of test and FE data to design model resistance based on a least squares analysis; V_δ is the CoV of the test and FE results relative to the design model; V_r is the combined CoV incorporating both model and basic variable uncertainties; γ_{M0} is the partial safety factor for cross-section resistance. Seen from this table, the resulting partial safety factors of the proposed CSM, the modified DSM as well as the Kato's method are 1.14, which are slightly greater than the recommend value:1.0 [107]. Despite that, they still present more satisfactory results than the existing design approaches (Eurocode 3 and AISC specification). The proposed expressions of the CSM, the DSM and the Kato's method are therefore recommended to be applied for the design of HSS I-section in bending.

Table 13 Reliability analysis results for design methods

Method	b	V_δ	V_r	γ_{M0}
EC3	1.106	0.051	0.097	1.15
AISC	1.015	0.120	0.146	1.23
CSM☆	1.041	0.044	0.093	1.14
DSM-AISI	1.106	0.048	0.096	1.14
DSM,mod☆	1.065	0.050	0.097	1.14
Kato☆	1.030	0.040	0.092	1.14

Note: the methods highlighted by "☆" in the figures are those ones newly developed in this study.

6 Conclusions

The continuous strength method (CSM), the direct strength method (DSM) and the method from Kato, developed with the incorporation of the flange-web interaction in I-section, have been extended to the design for local buckling behaviour of HSS I-sections under bending. Material properties test data for HSS materials were collated to capture the basic material properties for establishing the CSM material model for HSS. Bending test results of HSS I-section were gathered, and applied for validating the finite element model which was subsequently employed to generate numerical data for this study. The design expressions of the CSM, the DSM and the Kato's method for HSS I-section under bending were proposed based on an extensive parametric study, and assessed against the experimental and numerical results in comparison with the design rules in Eurocode 3 and AISC specification. HSSs with $f_{y,nom}$ = 460 MPa and $f_{y,nom}$ = 690-700 MPa were considered in the parametric study. The comparison results showed that all the design expressions, which are applicable to HSSs with $f_{y,nom}$ = 460-700 MPa, proposed in this study offer more accurate and less scattered predictions than the codified design rules. Also, attributing to the separate consideration of flange and web slenderness in the expression, the Kato's method provided more accurate strength predictions in comparison with the proposed CSM and the modified DSM. Besides, a reliability analysis in accordance with the standard evaluation procedure in EN 1990 was performed, demonstrating the satisfactory reliability level of the design expressions of proposed CSM, the modified DSM, the Kato's method.

Acknowledgements

The support from the Chinese National Engineering Research Centre for Steel Construction (Hong Kong Branch) at The Hong Kong Polytechnic University is gratefully acknowledged.

CRediT authorship contribution statement

Shuxian Chen: Investigation, Writing - original draft; *Han Fang:* Writing- review & editing. *Jun-zhi Liu*: Writing- review & editing; *Tak-Ming Chan*: Supervision, Funding acquisition.

Reference

[1] Shi, G. and Chen, X.S. (2018) Research advances in HSS structures at Tsinghua University and codification of the design specification. Steel Construction. 11(4), 286-293.

[2] Meng, X. (2020) Testing, simulation and design of high strength steel tubular elements. PhD thesis, Imperial College London. London, UK.

[3] Ban, H.Y. and Shi, G. (2018) A review of research on high-strength steel structures.

Proceedings of the Institution of Civil Engineers-Structures and Buildings. 171(8), 625-641.

[4] Baddoo, N. and Chen A.Q. (2020) High strength steel design and execution guide. SCI, Silwood Park, Ascot, Berkshire, UK.

[5] European Committee for Standardization (2005) EN 1993-1-1:2005, Eurocode 3: Design of steel structures - Part 1-1: General rules and rules for buildings. Brussels, CEN.

[6] American Institute of Steel Construction (2016) Specification for Structural Steel Buildings, ANSI/AISC 360-16. Chicago, Illinois, AISC.

[7] Beg, D. and Hladnik, L. (1996) Slenderness limit of class 3 I cross-sections made of high strength steel. Journal of Constructional Steel Research, 38(8), 201-207.

[8] Suzuki, T., Ogawa, T., Azuma, T. and Satsukawa, K. (1998) A study on large deformation behaviour of high strength steel beams with large depth−thickness ratio. Journal of Structural and Construction Engineering (Transactions of AIJ). 504, 95-101. (in Japanese)

[9] Ricles, J.M., Sause, R., Green, P.S. (1998) High-strength steel: implications of material and geometric characteristics on inelastic flexural behavior. Engineering Structures. 20(4~6), 323-335.

[10] Suzuki, T., Ogawa, T., Azuma, T. and Satsukawa, K. (1999) A study on plastic deformation capacity of 590 N/mm2 high strength steel beams with large depth−thickness ratio. Journal of Structural and Construction Engineering (Transactions of AIJ). 522, 113-119. (in Japanese)

[11] Tang, R.B. (2008) Plate yield slenderness criteria for structural members fabricated from high strength steels. PhD Thesis, Queensland University of Technology, Brisbane, Australia.

[12] Shi, Y.J., Xu, K.L., Shi, G. and Li, Y.X. (2018) Local buckling behavior of high strength steel welded I-section flexural members under uniform moment. Advances in Structural Engineering. 21(1), 93-108.

[13] Zhu, J.H. and Young, B. (2009) Design of aluminum alloy flexural members using direct strength method. Journal of Structural Engineering. 135(5), 558-566.

[14] Su, M.N., Young, B., Gardner, L. (2014) Testing and design of aluminum alloy cross sections in compression. Journal of Structural Engineering. 140(9), 04014047.

[15] Su, M.N., Young, B., Gardner, L. (2016) The continuous strength method for the design of aluminium alloy structural elements. Engineering Structures.122, 338–348.

[16] Afshan, S. and Gardner, L. (2013) The continuous strength method for structural stainless steel design. Thin-Walled Structures. 68, 42–49.

[17] Bock, M., Gardner, L., Real, E. (2015) Material and local buckling response of ferritic stainless steel sections. Thin-Walled Structures. 89,131–141.

[18] Huang, Y. and Young, B. (2018) Design of cold-formed stainless steel circular hollow section columns using direct strength method. Engineering Structures. 163, 177–183.

[19] Yun, X., Gardner, L., Boissonnade, N. (2018) The continuous strength method for the design of hot-rolled steel cross-sections. Engineering Structures. 157,179-191.

[20] Schafer, B.W. (2008) Review: The direct strength method of cold-formed steel member design. Journal of Constructional Steel Research. 64,766–778.

[21] Shifferaw, Y and Schafer, B.W. (2012) Inelastic bending capacity of cold-formed steel members. Journal of Structural Engineering. 138(4), 468-480.

[22] Lan, X.Y., Chen, J.B., Chan, T.K., Young, B. (2018) The continuous strength method for the design of high strength steel tubular sections in compression. Engineering Structures. 162 ,177-187.

[23] Lan, X.Y., Chen, J.B., Chan, T.K., Young, B. (2019) The continuous strength method for the design of high strength steel tubular sections in bending. Journal of Constructional Steel Research. 160, 499–509.

[24] Chen, J.B., Fang, H., Chan, T.M. (2021) Design of fixed-ended octagonal shaped steel hollow sections in compression. Engineering Structures. 228, 111520.

[25] Kato, B. (1998) Rotation capacity of H-section members as determined by local buckling. Journal of Constructional Steel Research. 13, 95-109.

[26] Kato, B. (1999) Deformation Capacity of Steel Structures. Journal of Constructional Steel Research. 17, 33-94.

[27] Architectural Institute of Japan (2010) Recommendation for Limit State Design of Steel Structures. Tokyo, AIJ.

[28] European Committee for Standardization (2005) EN 1990, Eurocode - Basis of structural design. Brussels, CEN.

[29] Wang, F. (2011) Study on mechanical performance of high strength steel and high strength steel frames. MSc Thesis, Chongqing University. Chongqing, China. (in Chinese)

[30] Shi, G., Wang, M., Bai, Y., Wang, F., Shi, Y.J., Wang, Y.Q. (2012) Experimental and modeling study of high-strength structural steel under cyclic loading. Engineering Structures. 37, 1-13.

[31] Lin, C.C. (2012) Local buckling and design method of high strength steel welded-section members under axial compression. MSc Thesis, Tsinghua University. Beijing, China. (in Chinese)

[32] Wei, C.X. (2013) Research on the structural performance and calculation model of Q460 high strength steel weld connection. MSc Thesis, Tsinghua University. Beijing, China. (in Chinese)

[33] Wang, J.J., Shi, G. and Shi, Y.J. (2014) Experimental research on behavior of 460 MPa high strength steel I-section columns under cyclic loading. Earthquake Engineering and Engineering Vibration.13, 611-622.

[34] Shokouhian, M. and Shi, Y.J. (2015) Flexural strength of hybrid steel I-beams based on slenderness. Engineering Structures. 93, 114–128.

[35] Xue, J.Y. (2014) Experimental research on the overall buckling behavior of high strength steel members under compression. MSc Thesis, Southeast University. Nanjing, China. (in Chinese)

[36] Liu, M. (2016) Research on the overall buckling behavior of axially compressed welded H-section columns made of Q460 high strength steel. MSc Thesis, Xi'an University of Architecture and Technology. Xi'an, China.

[37] Wang, J., Afshan, S., Gkantou, M., Theofanous, M., Baniotopoulos, C., Gardner, L. (2016) Flexural behaviour of hot-finished high strength steel square and rectangular hollow sections. Journal of Constructional Steel Research. 121, 97-109.

[38] Wang, J. and Gardner, L. (2017) Flexural buckling of hot-finished high-strength steel SHS and RHS columns. Journal of Structural Engineering. 143(6), 04017028.

[39] Bai, J.B. (2016) Research on the overall stability of Q460GJ welded h section beams. MSc Thesis, Chongqing University. Chongqing, China. (in Chinese)

[40] Duan, T. (2016) Study on residual stresses in welded moderate and heavy plate box sections made of Q460GJ steel. MSc Thesis, Chongqing University. Chongqing, China. (in Chinese)

[41] Nie, S.D. (2017) Study on overall stability load-carrying capacities of H-shaped and box section beam-columns welded by Q460GJ structural steel. PhD Thesis, Chongqing University. Chongqing, China. (in Chinese)

[42] Liu, P. (2017) Study on overall stability of welded Q460GJ steel axial compressed H-shaped Members. MSc Thesis, Chongqing University. Chongqing, China. (in Chinese)

[43] Zhu, Q. (2017) Experimental and model investigation on residual stresses in welded medium-walled and thick-walled I-shaped sections fabricated from Q460GJ. MSc Thesis, Chongqing University. Chongqing, China. (in Chinese)

[44] Hao, L.P. (2017) Experimental study on static and fatigue property of high strength steel welded joints. MSc Thesis, Xi'an University of Technology. Xi'an, China. (in Chinese)

[45] Xu, K.L. (2017) Local buckling behaviour and design method of high strength steel welded I-section beams. PhD Thesis, Tsinghua University. Beijing, China. (in Chinese)

[46] Chen, X.S. (2018) Seismic behavior and design method of high strength steel plate-reinforced beam-to-column joints. PhD Thesis, Tsinghua University. Beijing, China. (in Chinese)

[47] Hai, L.T., Sun, F.F., Zhao, C, Li, G.Q., Wang, Y.B. (2018) Experimental cyclic behavior and constitutive modeling of high strength structural steels. Construction and Building Materials 189, 1264-1285.
[48] Kang, S.B., Yang, B., Zhou, X., Nie, S.D. (2018a) Global buckling behaviour of welded Q460GJ steel box columns under axial compression. Journal of Constructional Steel Research.140, 153-162.
[49] Kang, S.B., Yang, B., Zhang, Y., Elchalakani, M., Xiong, G. (2018b) Global buckling of laterally-unrestrained Q460GJ beams with singly symmetric I-sections. Journal of Constructional Steel Research.145, 341-351.
[50] Yang, B., Zhang, Y. Xiong, G., Elchalakani, M., Kang, S.B. (2019) Global buckling investigation on laterally-unrestrained Q460GJ steel beams under three-point bending. Engineering Structures. 181, 271-280.
[51] Chen, J.B., Liu, H.X., Chan, T.M. (2020) Material properties and residual stresses of cold-formed octagonal hollow sections. Journal of Constructional Steel Research. 170, 106078.
[52] Li, J. (2020) Design method and overall buckling behaviour of Q460 high strength steel welded I-section simply-supported beams. MSc Thesis, Northeast Forestry University. Harbin, China. (in Chinese)
[53] McDermott, J.F. (1969) Plastic Bending of A514 Steel Beams. Journal of the Structural Division. 95(9), 1851-1871.
[54] Rasmussen, K.J.R. and Hancock, G.J. (1992) Plate slenderness limits for high strength steel sections. Journal of Constructional Steel Research. 23, 73-96.
[55] Yuan B. (1997) Local buckling of high strength steel W-shaped sections. MSc Thesis, McMaster University. Ontario, Canada.
[56] Salem, E.S. and Sause, R. (2004) Flexural strength and ductility of highway bridge I-girders fabricated from HPS-100W steel. ATLSS Reports. ATLSS report number 04-12:.
[57] Coelho, A.M.G., Bijlaard, F.S.K. and Kolstein, H. (2009) Experimental behaviour of high-strength steel web shear panels. Engineering Structures. 31, 1543-1555.
[58] Shi, G., Ban H.Y., Bijlaard, F. S. K., Shi, Y.J., Wang, Y.Q. (2011) Experimental study and finite element analysis on the overall buckling behavior of ultra-high strength steel compression members with end restraints. China Civil Engineering Journal. 44(10), 17-25. (in Chinese)
[59] Yan, J. B., Liew, J.Y.R., Zhang, M.H., Wang, J.Y. (2014) Mechanical properties of normal strength mild steel and high strength steel S690 in low temperature relevant to Arctic environment. Materials and Design. 61, 150-159.

[60] Chiew, S.P., Zhao, M.S., Lee, C.K. (2014) Mechanical properties of heat-treated high strength steel under fire/ post-fire conditions. Journal of Constructional Steel Research. 98, 12-19.

[61] Shi, Z.X. (2015) Local and local-overall buckling behavior of Q550 high strength steel welded members under axial compression. MSc Thesis, Southeast University. Nanjing, China. (in Chinese)

[62] Chen, S.W., Chen, X., Wang, Y.B., Lu, Z.L., Li, G.Q. (2016) Experimental and numerical investigations of Q690D H-section columns under lateral cyclic loading. Journal of Constructional Steel Research. 121, 268-281.

[63] Zhou, C. (2016) Research on local and local-overall buckling behavior of Q550 welded I-section members under axial compression. MSc Thesis, Southeast University. Nanjing, China. (in Chinese)

[64] Li, T.J., Li, G.Q., Chan, S.L., Wang, Y.B. (2016) Behavior of Q690 high-strength steel columns: Part 1: Experimental investigation. Journal of Constructional Steel Research.123, 18-30.

[65] Wang, Y.B., Li, G.Q., Sun, X., Chen, S.W., Hai, L.T. (2017b) Evaluation and prediction of cyclic response of Q690D steel. Proceedings of the Institution of Civil Engineers-Structures and Buildings. 170 (SB11), 788-803.

[66] Ma, T.Y., Hu, Y.F., Liu, X., Li, G.Q., Chung, K.F. (2017) Experimental investigation into high strength Q690 steel welded H-sections under combined compression and bending. Journal of Constructional Steel Research. 138, 449-462.

[67] Zhang, Y. (2017) Overall stability behaivor of Q690GJ welded H-shaped section beams. MSc Thesis, Southeast University. Nanjing, China. (in Chinese)

[68] Liu, X. (2017) Structural effects of welding onto high strength S690 steel plates and welded sections. PhD Thesis, The Hong Kong Polytechnic University. Hong Kong, China.

[69] Peng, Q. (2018) Investigation of flexural resistance and rotation capacity in Q690 high strength steel welded H-shaped flexural members. MSc Thesis, Southeast University. Nanjing, China. (in Chinese)

[70] He, B.B. (2018) Research on fire resistance performance of Rec-section Q550 high-strength steel columns with axial compression. MSc Thesis, Southeast University. Nanjing, China. (in Chinese)

[71] Wang, K. (2018) Study on structural behaviour of high strength steel S690 welded H- and I-sections. PhD Thesis, The Hong Kong Polytechnic University. Hong Kong, China.

[72] Huang, L., Li, G.Q., Wang, X.X., Zhang, C., Choe, L., Engelhardt, M. (2018) High temperature mechanical properties of high strength structural steels Q550, Q690 and Q890. Fire Technology. 54, 1609-1628.

[73] Ho, H.C., Liu, X., Chung, K.F., Elghazouli, A.Y., Xiao, M. (2018) Hysteretic behaviour of high strength S690 steel materials under low cycle high strain tests. Engineering Structures. 165, 222-236.

[74] Fang, H., Chan, T.M., Young, B. (2018) Material properties and residual stresses of octagonal high strength steel hollow sections. Journal of Constructional Steel Research.148, 479-490.

[75] Sun, Y., Liang, Y.T., Zhao, O. (2019) Testing, numerical modelling and design of S690 high strength steel welded I-section stub columns. Journal of Constructional Steel Research. 159, 521-533.

[76] Huang, Z.C., Li, D.X., Uy, B., Thai, H.T., Hou, C. (2019) Local and post-local buckling of fabricated high-strength steel and composite columns. Journal of Constructional Steel Research. 154, 235-249.

[77] Lai, B.L., Liew, J.Y.R., Hoang, A.L. (2019) Behavior of high strength concrete encased steel composite stub columns with C130 concrete and S690 steel. Engineering Structures. 200, 109743.

[78] Sun, Q., Qu, S.Z., Wu, X.H. (2019) Ultimate load capacity analysis of Q690 high-strength steel KK-type tube–gusset plate connections. Journal of Structural Engineering. 145(8), 04019074.

[79] Ho, H.C., Chung, K.F., Liu, X., Xiao, M., Nethercot, D.A. (2019) Modelling tensile tests on high strength S690 steel materials undergoing large deformations. Engineering Structures.192, 305-322.

[80] Amraei, M., Ahola, A., Afkhami, S., Björk, T., Heidarpour, A., Zhao, X.L. (2019) Effects of heat input on the mechanical properties of butt-welded high and ultra-high strength steels. Engineering Structures. 198, 109460.

[81] Zhang, L.L., Wang, F.Y., Liang, Y.T., Zhao, O. (2019) Press-braked S690 high strength steel equal-leg angle and plain channel section stub columns: Testing, numerical simulation and design. Engineering Structures. 201, 109764.

[82] Le, T. Bradford, M.A., Liu, X.P., Valipour, H.R. (2020) Buckling of welded high-strength steel I-beams. Journal of Constructional Steel Research. 168, 105938.

[83] Guo, Y.B., Ho, H.C., Chung, K.F., Elghazoulic, A.Y. (2020) Cyclic deformation characteristics of S355 and S690 steels under different loading protocols. Engineering Structures. 221, 111093.

[84] Su, A.D., Sun, Y., Liang, Y.T., Zhao, O. (2020) Material properties and membrane residual stresses of S690 high strength steel welded I-sections after exposure to elevated temperatures. Thin–Walled Structures.152, 106723.

[85] Ho, H.C., Xiao, M., Hu, Y.F., Guo, Y.B., Chung, K.F., Yama, M.C.H., Nethercot, D.A. (2020) Determination of a full range constitutive model for high strength S690 steels. Journal of Constructional Steel Research.174, 106275.

[86] Hu, Y.F., Chung, K.F., Ban, H.Y., Nethercot, D.A. (2020) Investigations into residual stresses in S690 cold-formed circular hollow sections due to transverse bending and longitudinal welding. Engineering Structures. 219, 110911.

[87] Zhang, C.T., Wang, R.H., Song, G.B. (2020) Effects of pre-fatigue damage on mechanical properties of Q690 high strength steel. Construction and Building Materials. 252, 118845.

[88] Cadoni, E. and Forni, D. (2020) Strain-rate effects on S690QL high strength steel under tensile loading. Journal of Constructional Steel Research. 175, 106348.

[89] Chung, K. F., Ho, H.C., Hu, Y.F., Wang, K., Liu, X., Xiao, M., Nethercot, D.A. (2020) Experimental evidence on structural adequacy of high strength S690 steel welded joints with different heat input energy. Engineering Structures. 204, 110051.

[90] Wang, F. and Lui, E.M. (2020) Experimental study of the post-fire mechanical properties of Q690 high strength steel. Journal of Constructional Steel Research. 167, 105966.

[91] Chen, J.B. and Chan, T.M. (2020) Material properties and residual stresses of cold-formed high-strength-steel circular hollow sections. Journal of Constructional Steel Research.170, 106099.

[92] Lin, X.M., Yam, M.C.H., Chung, K.F., Lam, A.C.C. (2021) A study of net-section resistance of high strength steel bolted connections. Thin–Walled Structures. 159,107284.

[93] Yang, B., Dong, M.H., Han, Q., Elchalakani, M., Xiong, G. (2021) Flexural behavior and rotation capacity of welded I-beams made from 690-MPa high-strength steel. Journal of Structural Engineering. 147(2), 04020320.

[94] Bartsch, H., Eyben, F., Pauli, G., Schaffrath, S., Feldmann, M. (2021) Experimental and numerical investigations on the rotation capacity of high-strength steel beams. Journal of Structural Engineering. 147(6), 04021067.

[95] Ban, H.Y., Shi, G., Shi, Y.J., Bradford, M.A. (2013) Experimental investigation of the overall buckling behaviour of 960 MPa high strength steel columns. Journal of Constructional Steel Research. 88, 256-266.

[96] Qiang, X.H., Bijlaard, F.S.K., Kolstein, H. (2013) Post-fire performance of very high strength steel S960. Journal of Constructional Steel Research. 80, 235-242.

[97] Cadoni, E. and Forni, D. (2019) Mechanical behaviour of a very-high strength steel (S960QL) under extreme conditions of high strain rates and elevated temperatures. Fire Safety Journal. 109,102869.

[98] Li, D.X., Huang, Z.C., Uy, B., Thai, H.T., Hou, C. (2019) Slenderness limits for fabricated S960 ultra-high-strength steel and composite columns. Journal of Constructional Steel Research. 159, 109-121.

[99] Amraei, M., Afkhami, S., Javaheri, V., Larkiola, J., Skriko, T., Björk, T., Zhao, X.L. (2020) Mechanical properties and microstructural evaluation of the heat-affected zone in ultra-high strength steels. Thin–Walled Structures. 157, 107072.

[100] Wang, W.Y., Zhang, Y.H., Li, X. (2020a) Experimental study on mechanical properties of high strength Q960 steel after high temperature. Journal of Building Materials. Aavailable from:
https://kns.cnki.net/kcms/detail/31.1764.TU.20201118.1800.022.html (in Chinese)

[101] Wang, F.Y., Zhao, O., Young, B. (2020b) Testing and numerical modelling of S960 ultra-high strength steel angle and channel section stub columns. Engineering Structures. 204, 109902.

[102] Lan, X.Y., Chan, T.M., Young, B. (2020) Experimental study on the behaviour and strength of high strength steel CHS T- and X-joints. Engineering Structures. 206, 110182.

[103] Su, A.D., Liang, Y.T., Zhao, O. (2021) Experimental and numerical studies of S960 ultra-high strength steel welded I-section columns. Thin–Walled Structures. 159, 107166.

[104] Green, P.S., Sause, R., Ricles, J.M. (2002) Strength and ductility of HPS flexural members. Journal of Constructional Steel Research. 58, 907-941.

[105] Lee, C.H., Han, K.H., Uang, C.M., Kim, D.K., et al. (2013) Flexural strength and rotation capacity of I-shaped beams fabricated from 800-MPa Steel. Journal of Structural Engineering. 139(6), 1043-1058.

[106] Sun, Y., He, A., Liang, Y.T. and Zhao, O. (2019) In-plane bending behaviour and capacities of S690 high strength steel welded I-section beams. Journal of Constructional Steel Research. 162,105741.

[107] European Committee for Standardization (2006) EN 1993-1-5:2006. Eurocode 3 - Design of steel structures - Part 1-5: Plated structural elements. Brussels, CEN.

[108] Ban, H.Y., Shi, G., Shi, Y.J. (2014) Experimental and unified model investigations on residual stress within high strength steel welded I-sections. Engineering Mechanics. 31(8), 83-91. (in Chinese)

[109] Ma, J.L. (2016) Behaviour and Design of Cold-Formed High Strength Steel Tubular Members. PhD Thesis, The University of Hong Kong, HK, China.

[110] British Standards Institution (2017) BS EN 10365:2017. Hot rolled steel channels, I and H sections - Dimensions and masses. London, BSI.

[111] Gardner, L. and Nethercot, D. A. (2004) Structural stainless steel design: A new approach. The Structural Engineer. 82(21), 21-28.

[112] Buchanan, C., Gardner, L., Liew, A. (2016) The continuous strength method for the design of circular hollow sections. Journal of Constructional Steel Research.118, 207–216.

[113] Zhao, O., Afshan, S., Gardner, L. (2017) Structural response and continuous strength method design of slender stainless steel cross-sections. Engineering Structures.140, 14-25.

[114] Yun, X. and Gardner, L. (2017) Stress-strain curves for hot-rolled steels. Journal of Constructional Steel Research.133, 36-46.

[115] European Committee for Standardization (2007) EN 1993-1-12:2007. Eurocode 3 - Design of steel structures - Part 1-12: Additional rules for the extension of EN 1993 up to steel grades S 700. Brussels, CEN.

[116] Sadowski, A.J., Rotter, J.M., Reinke, T., Ummenhofer, T. (2015) Statistical analysis of the material properties of selected structural carbon steels. Structural Safety. 53, 26–35.

[117] Schafer, B.W. and Pekoz, T. (1998) Direct strength prediction of cold-formed steel members using numerical elastic buckling solutions. In: Proceedings of the fourteenth international specialty conference on cold-formed steel structures, St. Louis, Missouri U.S.A., October 15-16, 1998. University of Missouri – Rolla. pp. 69–76.

[118] American Iron and Steel Institution (2016) North American specification for the Design of cold-formed steel structural members, AISI S100-16. Washington, D.C., AISI.

[119] Afshan, S., Francis, P., Baddoo, N.R., Gardner, L. (2015) Reliability analysis of structural stainless steel design provisions. Journal of Constructional Steel Research. 114,293–304.

[120] Aluminium Association. (2010). Aluminium design manual AA ADM-2010, Washington, DC., AA.